Nano Energy 118 (2023) 108969

Contents lists available at ScienceDirect

Nano Energy

journal homepage: www.elsevier.com/locate/nanoen

Review

The ferro-pyro-phototronic effect for high-performance self-powered photodetectors

Ampattu Ravikumar Jayakrishnan [a,1], José P.B. Silva [b,c,*], Katarzyna Gwozdz [d], Maria J. M. Gomes [b,c], Robert L.Z. Hoye [e], Judith L. MacManus-Driscoll [f,**]

[a] Department of Physics, Sree Narayana Guru College of Advanced Studies, Alappuzha 690513, India
[b] Physics Center of Minho and Porto Universities (CF-UM-UP), University of Minho, Campus de Gualtar, 4710-057 Braga, Portugal
[c] Laboratory of Physics for Materials and Emergent Technologies, LapMET, University of Minho, 4710-057 Braga, Portugal
[d] Department of Quantum Technologies, Wroclaw University of Science and Technology, Wroclaw 50-370, Poland
[e] Inorganic Chemistry Laboratory, Department of Chemistry, University of Oxford, South Parks Road, Oxford OX1 3QR, UK
[f] Dept. of Materials Science and Metallurgy, University of Cambridge, 27 Charles Babbage Rd., Cambridge CB3 OFS, UK

ARTICLE INFO

Keywords:
Self-powered photodetectors
Ferro-pyro-phototronic effect
IoT applications

ABSTRACT

Self-powered photodetectors are advantageous over conventional photodetectors because they can have outstanding performance in the absence of an external power source, which is important for a range of applications, including in the Internet of Things. Current research has demonstrated different types of self-powered photodetectors utilizing the photovoltaic effect, pyroelectric effect, piezoelectric effect, and synergic effects, such as the piezo-phototronic and pyro-phototronic effects. Such effects have been demonstrated in standard semiconductors, in hybrid inorganic-organic halide perovskites and in all inorganic perovskites. Very recently, a novel type of self-powered photodetector exploring the coupling between the photovoltaic, the pyroelectric and the ferroelectric effects (i.e., ferro-pyro-phototronic effect) has attracted great interest, owing to the excellent photo current response achieved with this triple coupling. The ferro-pyro-phototronic effect can therefore be an important route towards improving the performance of self-powered photodetectors. Since ferroelectricity has the potential to bring revolutionary changes in many contemporary technologies, including non-volatile memory, solar cells, field effect transistors, energy storage, and energy harvesters, it is worthwhile exploring in more detail how the ferroelectric effect enhances the triple coupling. Thus, this focus review covers the research conducted so far on the ferro-pyro-phototronic effect, discussing recent progress on the development of self-powered photodetectors based on this effect, and also highlighting current challenges and potential solutions for using these devices in real-world applications.

1. Introduction

After the discovery of the photoelectric effect more than one century ago, photodetectors (PDs) that can convert radiation into electronic signals were developed [1,2]. A PD works on the principal of converting a light signal into electric current that can be further processed or stored. Based on the optical signal wavelength from ultraviolet (UV), visible, and near-infrared (NIR) regions, distinct types of PDs are employed over the electromagnetic spectrum [3]. The key parameters that determine the performance of PDs are the ON/ OFF ratio (ratio between the photocurrent under light and dark conditions), the response time (corresponding to the ON and OFF state of light known as the rise time (ON state) and the fall time (OFF state)), the cut-off frequency, the responsivity (photocurrent extracted from the device per unit per unit power of light), and the specific detectivity (how efficiently the device detects light) [3–5]. However, recent investigations have concentrated on developing PDs operating *without* an external power source (also known as self-powered photodetectors). The ability of a PD to self-power is extremely important as this means low energy consumption and a much smaller size, enabling the possibility of device fabrication at the

* Corresponding author at: Physics Center of Minho and Porto Universities (CF-UM-UP), University of Minho, Campus de Gualtar, 4710-057 Braga, Portugal.
** Corresponding author.
E-mail addresses: josesilva@fisica.uminho.pt (J.P.B. Silva), jld35@cam.ac.uk (J.L. MacManus-Driscoll).
[1] Present address: Physics Center of Minho and Porto Universities (CF-UM-UP), University of Minho, Campus de Gualtar, 4710-057 Braga, Portugal.

https://doi.org/10.1016/j.nanoen.2023.108969
Received 29 June 2023; Received in revised form 11 September 2023; Accepted 3 October 2023
Available online 5 October 2023

nanoscale [3,4]. Currently, to enhance the performance of self-powered PDs, materials with improved features of high speed, high stability, high signal-to-noise (S/N) ratio, and high sensitivity, over a wide range of wavelengths, from UV to visible to IR, are the focus of research community. Such high performance self-powered PDs are prospective contenders for a very wide variety of applications [3–7].

1.1. Self-powered photodetectors: importance and current developments

Self-powered photodetectors (SPDs) are important for IoT devices, smart wearable electronics, robotics, health monitoring, human-machine interfaces, image sensors, wireless control systems, and more broadly across life sciences [2–7]. IoT, in particular, is a very important and fast-growing field (projected to grow from $662.21 billion in 2023 to $3352.97 billion by 2030, at a CAGR of 26.1%) in areas like environment monitoring, traffic control, and logistics. Such applications require high performance SPDs in the UV and visible wavelength range (UV–Vis) as sensors to convert optical signals to electrical signals for optical wireless communications [6,8]. Here, in conventional PDs, photogenerated electrons and holes/ charge carriers are separated to generate electric current, and this require power, via a battery power source, are complex, inefficient, costly, increase the size of the devices, and require high maintenance. We note the device size is a crucial factor for easy movement of the device and for enabling long-term stand-alone installation in large-scale networks [3,4]. SPDs could revolutionize next-generation IoT in terms of size, weight, and power consumption. An ideal SPD would have a simple structure, be made of non-hazardous chemicals, be maintenance free, have zero or low power consumption, provide wireless operation, be durable, and would exist in harsh environments [3,4].

Further selection criteria of a material for a UV–Vis SPD is that it has a wide band gap (~1.8–3.4 eV), fast response time, and the possibility to be miniaturized [7]. ZnO, TiO_2, ZnS, MoS_2, GaN, CdS semiconductor materials have attracted significant attention. Also, recently, low-dimensional semiconductor nanostructures have been shown to be ideal candidates for light detection owing to their ultrafast response times, excellent responsivity, and good detection capability [7]. Further, nano-structured SPD materials offer merits such as small size enabling easy miniaturization, reduced weight, and low power consumption [4]. Different sophisticated device fabrication methods such as atomic layer deposition (ALD), magnetron sputtering, pulsed laser deposition, chemical vapour deposition (CVD), molecular beam epitaxy (MBE), etc. have been employed for the fabrication of nanostructured UV–Vis SPDs [4]. The working mechanisms and summary of experimental investigations on semiconductor SPDs has been reviewed in detail before [3–5,9,10]. Particularly, the exploration of ZnO based SPDs has been extensive with different phenomena involved, including the photovoltaic, pyroelectric, piezoelectric, and pyro-phototronic effects (PPE). ZnO is the 'champion' material due to its chemical simplicity, good chemical and radiation stability and, low ratio of hole and electron ionization coefficient (which allows fast and low-noise avalanche photodetection in the UV spectral range) [9–12]. In addition, ZnO has a strong exciton transition near the electronic band gap and an electron-hole binding energy of 60 meV, and the optical properties are dominated by strong light-matter interaction, involving exciton polaritons. Not only is ZnO a good material for UV SPDs, it shows good broad band photodetection in the visible, and IR regions [9,10]. Fig. 1 shows the best performance achieved in ZnO based SPDs to date [11,12].

1.2. An overview of the pyro-phototronic effect and semiconductor self-powered photodetectors

Electric current generation via the photovoltaic effect (PVE) in UV–Vis PDs has been explored in a wide variety of materials beyond ZnO, e.g. TiO_2, GaN, CdS, MoS_2, InSe and Ga_2O_3. [3,4,7,9]. Some of these materials overlap with the aforementioned ones (Section 1.1),

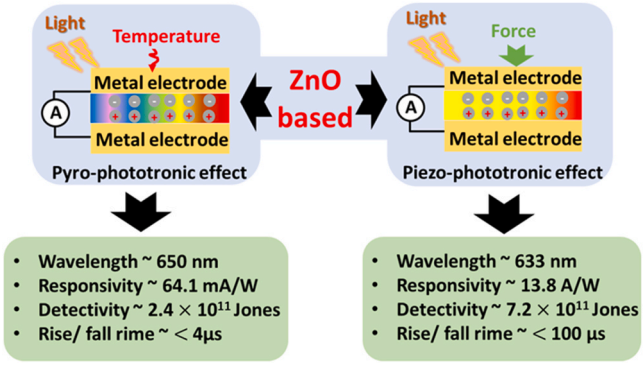

Fig. 1. Best performance achieved in ZnO based SPDs [11,12].

which are excellent materials for SPD. In PVE-SPDs, the light induced electron and hole pair separation is enabled by the work function difference at a metal/ semiconductor Schottky barrier (SB) or at a semiconductor p-n junction (Fig. 2**a**) [10]. However, both provide a relatively weak intrinsic internal electric field to separate the photoexcited electron-hole pair [9], and so the photoresponsivity is relatively low. Thus, to increase the internal field, an additive pyroelectric effect from non-centrosymmetric semiconductor (NCS) materials at p-n heterojunctions has been explored (Fig. 2**b**) [9]. Hence, the pyro-phototronic effect (PPE) has been successfully achieved, with high photocurrent demonstrated in ZnO SPDs [9–14]. Polar ZnO is pyroelectric because thermal fluctuations induced by any incident light produces a spontaneous polarization change in the material. Therefore, the negative and positive charge separation in the ZnO produces a field which is in the same direction as the built in field at the p-n junction. This promotes photogenerated charge carrier separation above what the relatively weak built in field does and thus increases the photocurrent. Also, the SB height is lowered by the pyroelectric charge, and this builds up a pyroelectric potential at the metal/NCS interface which promotes charge-carrier transport into the metal, which gives a further boost to the photocurrent [10]. This phenomenon is known as the pyro-phototronic effect. Further increases in the light intensity induces a thermal strain across the NCS due to an increase in the temperature. This leads to a polarization change due to the piezoelectric effect known as secondary pyroelectric effect [15]. A pyroelectric material undergoing thermal change experiences an electric displacement via thermal expansion and compression inducing a piezoelectric potential. As a result, electron flow takes place through the external circuit signifying the pyroelectric effect. This phenomenon is known as a secondary pyroelectric effect [15]. Consequently, the metal/NCS behaves as an ohmic-like contact with a reduced SB height, and thereby boosts photocurrent response (Fig. 2**c**) [9,10]. In this way, high intensity illumination on NCS brings out a combined effect comprising of the pyroelectric and secondary pyroelectric effect, as well as the photovoltaic effect by controlling the charge transport across the metal/NCS interface.

Furthermore, the internal electric field in a photoexcited NCS can be effectively enhanced by applying an external strain. This phenomenon is known as the piezo-phototronic effect [16–19]. The application of an external strain induces a piezoelectric polarization that boosts the separation of the photo-excited electrons and holes, which in turn contributes to the transfer of the photoexcited charge carriers. The strain-induced ionic polarisation in the non-centrosymmetric semiconducting crystal produces the piezo potential, which acts as a 'gate' voltage to adjust or regulate the charge-carrier transport across the metal-semiconductor interface or the p-n junction [16–19]. Thus, the piezo-phototronic effect utilizes the piezoelectric, photoexcitation, and semiconducting properties for controlling the charge generation, separation/ and or recombination, and charge transport to optimise the performance of the optoelectronic devices.

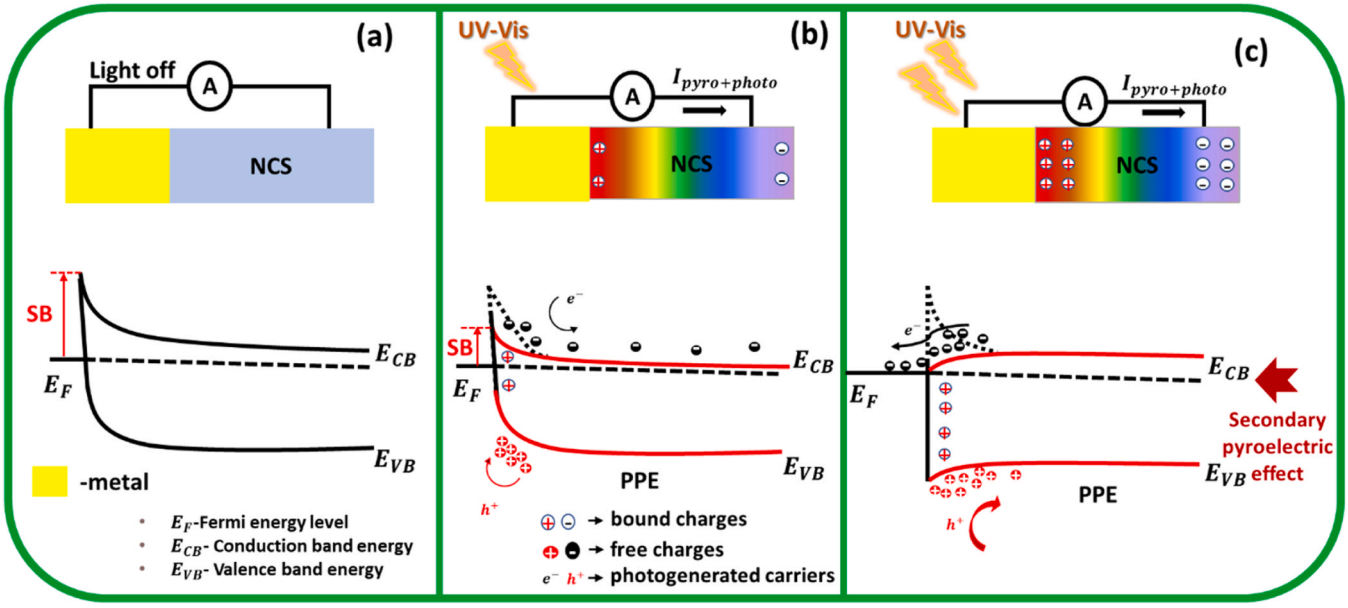

Fig. 2. Working mechanism of Non-Centro Symmetric semiconductors (NCS) in Creating the Pyro-Phototronic Effect (PPE).

Metal halide perovskites (MHP) semiconductors, well known for their excellent solar cell and light emitting diode performance [13,14] have also been shown to have a wide sensing range from the UV–Visible-NIR region to the gamma region comparable to inorganic semiconductor oxides [15]. These materials have a particularly long carrier lifetime, superior absorption co-efficient, tuneable optical properties, and ease of fabrication [13,14]. However, it is not our aim to review the work developed on SPD based on pyro-phototronic effect and piezo-phototronic effect as this has already been well covered in the earlier reviews [3–5,9–12,17,18].

The key aim of this review is to analyze and discuss the emerging use of the ferro-pyro-phototronic effect for enhancing the performance of SPDs. This review starts with an introduction about photodetectors. Next, the review highlights the importance of self-powered photodetectors (SPDs) and it discusses recent developments in this field. A brief explanation of the different mechanisms responsible for photodetection in SPDs, namely the influences of the photovoltaic effect, pyro-phototronic effect, and piezo-phototronic effect then follows. Finally, the exemplary SPD performance arising from the novel FPPE effect is included as well as current developments and challenges for this topic.

1.3. Introduction to the ferro-pyro-phototronic effect

The discovery of the PVE in ferroelectric (FE) materials half a century ago paved the way to stable photovoltage and photocurrent responses suitable for PDs [1,2]. Even though ferroelectrics have seldom been explored for SPDs, there have been several recent investigations into two-dimensional (2D) metal-halide based perovskites materials and inorganic ABO_3 perovskites (such as barium titanate ($BaTiO_3$/ BTO), lead zirconate titanate ($Pb(Zr, Ti)O_3$/ PZT), and bismuth ferrite ($BiFeO_3$/ BFO), etc.) in SPD devices [10].

Inorganic perovskite FEs have higher pyroelectric and piezoelectric coefficients than other semiconductors (such as ZnO, TiO_2, etc.) and hence the SPD response can be tuned by controlling the ferroelectric polarization, leading to a high output current under UV–Vis light illumination [19]. **Pyroelectric FEs are fascinating owing to the simultaneous response to electric-thermal conditions recovering enhanced photocurrent. Such a high photocurrent response in FE is attributed to the large driving force induced by the superior pyroelectric coefficient and intrinsic ferroelectricity, which augment the inner electric field to significantly enhance the electron and hole separation under light illumination. This large driving force arises from the depolarization field due to photovoltaic effect, which is attributed to the incomplete ferroelectric polarisation charge screening**. In view of this, we believe ferroelectricity induced PPE or so called **ferro-pyro-phototronic effect (FPPE)** can be crucial in the next generation SPDs (Fig. 3). More effort has recently been put on comprehending new materials in this area utilizing the ferro-pyro-phototronic effect [19–28]. In this focus review article, we compare the performance metrics of various ferroelectric materials in the FPPE. Table 1 shows a comparison of performance of FE based PDs utilizing the FPPE [19–26]. We start with established systems and then moves to discussing new FE based systems which could enhance the FPPE above current systems. We also provide our own perspective on the design FE based high-performance SPDs.

2. Fundamentals of the ferro-pyro-phototronic effect

NCS in SPDs often have low pyroelectric coefficient and weak PVE (and hence low built-in electric field), and therefore do not effectively separate photogenerated electrons and holes, leading to poor performance. [13,19]. As discussed in the previous section (Section 1.3), ferroelectric (FE) NCS materials can be exploited in SPDs for their ferroelectric, pyroelectric, and piezoelectric properties, with each phenomenon enhancing SPD performance. Thus, FE-based SPD offer a multi-functional effect. Very recent investigations revealed a general working mechanism of the FPPE in FE-based systems, as shown in Fig. 4. Before subjecting the FE SPD to UV–Vis light illumination, the FE material is poled to induce ferroelectricity. The performance of the FE SPD differs under dark and light conditions (Fig. 4**a** compared to Fig. 4**b**), and under either simultaneous 'light + heating'(c) or 'light + cooling' (d) conditions.

Under dark conditions, the FE layer will be trapped between the two Schottky barriers (SB) with work functions ϕ_{d} and ϕ_{s}, respectively as shown in Fig. 4**a**. When the FE is poled and subjected to a weak UV–Vis light irradiation, the charges will be separated at the interfaces as shown in the Fig. 4**b**. This leads to a SB height difference in such a way that ϕ_{d-1} decreases (left interface) and ϕ_{s-1} (right interface) increases. Upon UV 'light + heating' (Fig. 4**c**), the SB changes as ϕ_{d-2} increases (left interface) and ϕ_{s-2} (right interface) increases. As the intensity of the light increases, the coupling effect of the FE saturation polarization, pyroelectric effect and thermal strain induced (piezoelectric) secondary

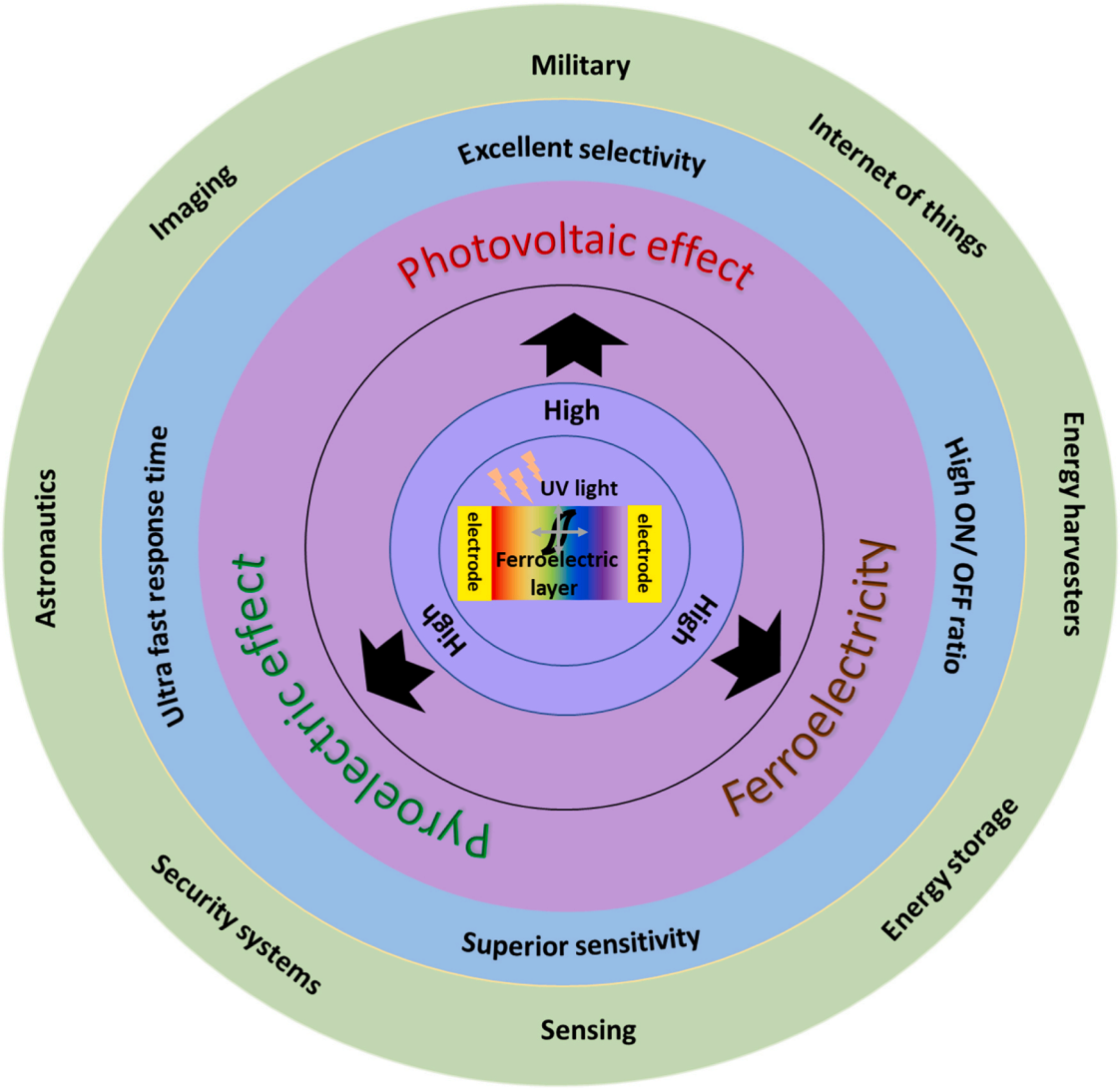

Fig. 3. Overview of the advantages and potential impact of ferro-pyro-phototronic effect-based ferroelectric self-powered photodetectors.

Table 1
Comparison of the performance of different ferroelectric self-powered photodetectors utilizing ferro-pyro-phototronic effect.

Device structure	FE class	Illumination (nm)	Response time (μs)		Detectivity (10^{10} Jones)	Responsivity (mA/W)	Ref
			Rise	Fall			
<Ag/Bi/$(PMA)_2PbCl_4$ MMB/Bi/Ag>	Halide	320	162	226	10.1	9000	[20]
<Ag/Bi/$(PMA)_2PbCl_4$ SCM/Bi/Ag>	Halide	320	73	52	0.00023	155.5	[21]
<PEN/ITO/TMIMPbI_3-MAPbI_3 P3HT/Ni/Au>	Halide	532	35000	36000	0.5	6.6	[22]
<ITO/$(BA)_2MA_3Pb_4Br_{13}$/ PC61BM/Bi/Ag>	Halide	360	260	420	1.54×10^4	1×10^3	[23]
<ITO/BTO/ITO>	FE ceramics	405	-	-	0.00159	0.0014	[24]
<Ag/BNT/ITO>	FE ceramics	405	84200	54300	-	-	[25]
<Al/Si/SiO_x/BCZT/ITO>	FE thin film	405	2.4	1.5	1.7	13.1	[26]
<ITO/Bi@$Bi_{3.8}Nd_{0.2}Ti_3O_{12}$/Al>	FE thin film	390	57	114	81.1	159	[27]
<Ti/Au/α-In_2Se_3/n-Si/In/Ga>	FE semiconductor film	405	43	12	1600	560	[28]

* $BaTiO_3$-BTO, $Bi_{0.5}Na_{0.5}TiO_3$-BNT, $0.5Ba(Zr_{0.2}Ti_{0.8})O_3$-$0.5(Ba_{0.7}Ca_{0.3})TiO_3$- BCZT.

pyroelectric effect contributes to the photocurrent. This phenomenon is the FPPE. During 'light + cooling', again the SB height modulates to ϕ_{d-3} (at the left interface decreases) and ϕ_{s-3} (at the right interface increases) as shown in Fig. 4**d** [19,20]. As a result, the barrier height ϕ_{s-3} strengthen electron-hole pair separation (because the polarized charges increase with decrease in temperature) and the barrier height ϕ_{d-3} accelerates the electron flow. This will also promote the photocurrent response via the FPPE. In this way, a high performance self-powered FE based PD is developed by tailoring the energy band diagram. In fact, the pyroelectric and secondary pyroelectric features can be utilized more in FE SPDs to enhance the photocurrent than in NCS SPDs, which makes them potential candidates for energy harvesting applications as well as for SPDs. Thus, the FE SPDs could become a game changer in future optoelectronic applications.

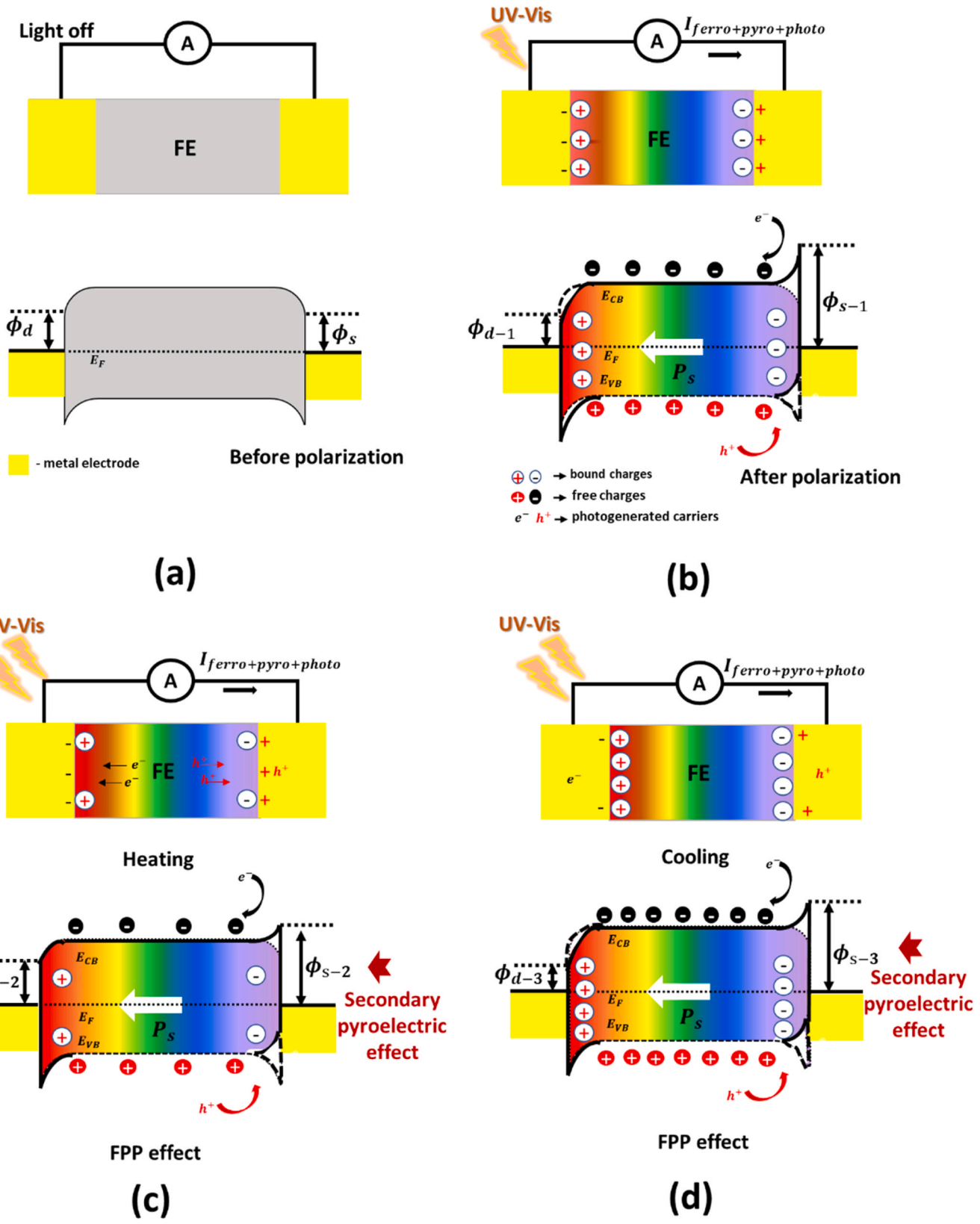

Fig. 4. Working mechanism of ferroelectrics in semiconductor photodiodes explained in terms of energy band diagrams, band bending and carrier generation and drift.

3. Recent advances in the use of the ferro-pyro-phototronic effect in self-powered photodetectors

In this section, we discuss the different types of FE materials utilizing the FPPE for self-powered photodetection, specifically concentrating on the materials, their fabrication methods, and their performance in SPD devices.

3.1. Metal halide-based perovskites

Metal halide perovskites (MHPs) such as $(PMA)_2PbCl_4$ (PMA = benzylammonium), $(BA)_2(MA)_2Pb_3Cl_{10}$ (BA = $C_4H_9NH_3^+$), and $(EA)_2Pb_3Cl_{10}$ (EA = ethylammonium) exhibit very good optoelectronic properties due to low trap density, high charge-carrier mobilities along the in-plane direction, and high optical absorption coefficients [13]. In addition, 2D lead-halide perovskites have intrinsic ferroelectric and pyroelectric properties with unique structure and tunability, which is beneficial for self-powered PDs [13,14]. These 2D materials, therefore, serve as an ideal platform for self-powered PDs via the FPPE. Very recently Guo et al. created a 2D halide ferroelectric $(PMA)_2PbCl_4$ monocrystalline microbelt (MMB) UV SPD. A novel method called space-confined assisted antisolvent growth was used to synthesize the MMB, as shown in Fig. 5**a** [20]. Initially, a $(PMA)_2PbCl_4$ precursor solution was dropped onto to a Si/SiO_2 substrate and another Si/SiO_2 substrate of same size was placed on top of the precursor solution. This set up was clamped and a large pressure applied by adjusting the clamp. Finally, the set-up was placed in a sealed dessiccator containing anisole solvent (maintained at 40 ^oC) for the $(PMA)_2PbCl_4$ MMB growth (Fig. 5**a**). X-ray diffraction (XRD) confirmed polycrystalline $(PMA)_2PbCl_4$ (Fig. 5**b**) and an orthorhombic structure of $(PMA)_2PbCl_4$ was elucidated with the help of selected area electron diffraction (SAED) indicating the MMB's growth direction along [011] direction (Fig. 5**c**). Further, the performance of the MMBs array was determined by transferring the patterned $(PMA)_2PbCl_4$ arrays onto a flexible polyethylene naphthalate (PEN) substrate with Bi/Ag electrode pairs. Initially, a SB was formed between the $(PMA)_2PbCl_4$ microbelts and Bi/Ag electrodes. The device was subjected to electric field poling before the photoresponse studies. During illumination with 320 nm wavelength light, a photocurrent was generated in the perovskite array. The device showed a high responsivity (9000 mA/ W) and detectivity (1×10^{11} Jones) with a very good response time. The reported responsivity was 128 times higher compared to photoexcitation alone. Moreover, the unencapsulated device has been tested under harsh environment such as high humidity, thermal environment, and intense laser illumination, showing a stable operation. Such stability against a harsh environment arises due to the presence of a Bi interlayer which acts as an effective barrier to the permeation. The strong performance of the device can be explained by the influence of the FPPE (as was shown schematically in Fig. 4). Hence, under illumination in the absence of heat, there absorption of light and consequent separation of electron-hole pairs via the built-in electric field. However, there is a temperature rise caused by the light illumination, which leads to a pyroelectric current. Also, the temperature rise causes the energy band edge of the $(PMA)_2PbCl_4$ MMBs to bend downwards due to ferroelectric polarization charge (or ferroelectric-induced bound charges) induced by the pyroelectric effect. Hence, electrons move towards the SB interface, while the holes move away from SB interface. Thus, the SB interface was controlled to suppress the separation of the light generated charge carriers, thus enhancing the output current from the FPPE. Overall, these FPPE coupled SPDs based on 2D MHP, exhibit stable and high photo detection performance compared to

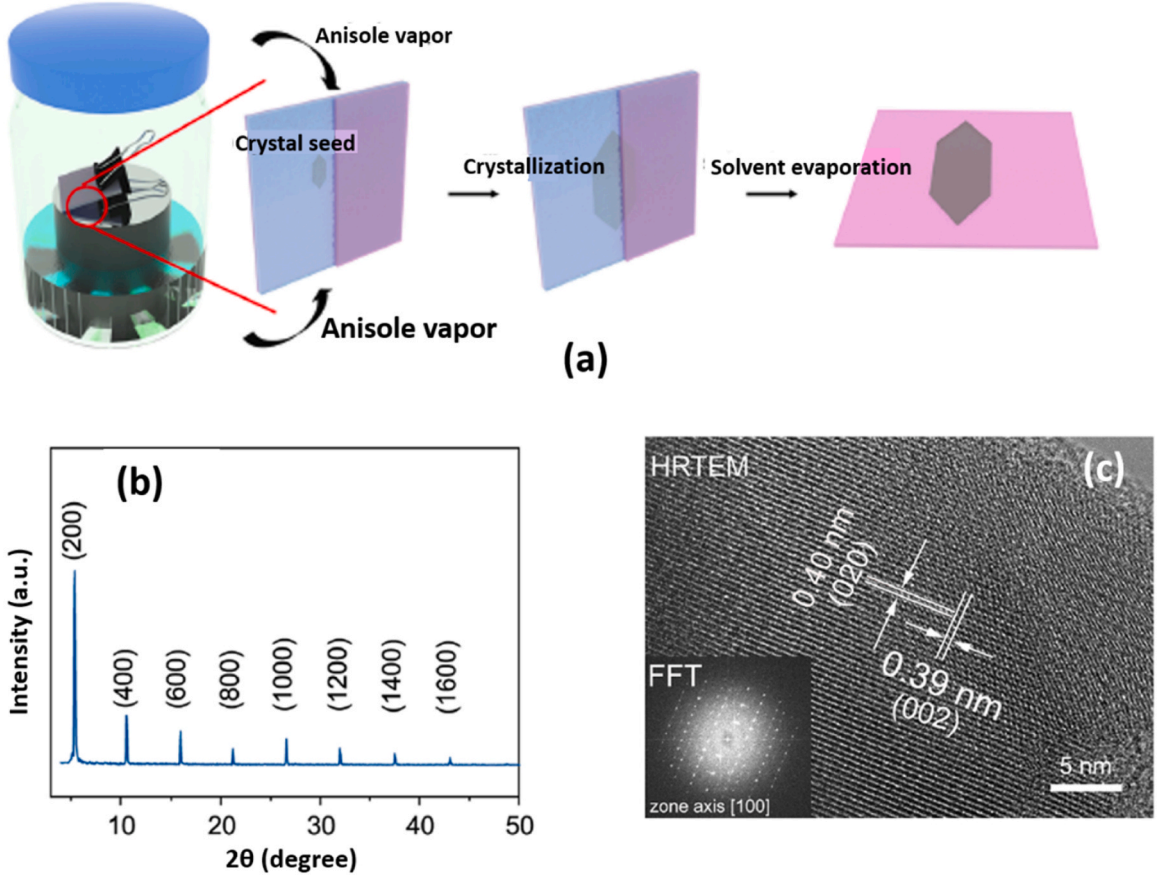

Fig. 5. (a) Preparation, (b) XRD pattern, and (c) seleted area electron diffraction pattern of 2D halide ferroelectric $(PMA)_2PbCl_4$ MMB. Reproduced with permission [20]. Copyright@ 2022, American Chemical Society Publishing.

semiconductor SPDs [20].

It should be noted when discussing the specific detectivity of these PDs and other emerging PDs that the noise current was not directly measured in many cases, and the authors do not go into details into how exactly the D^* values were derived. Typically, it is assumed that the noise current is only due to shot and thermal noise, but this can lead to D^* being over-estimated because of an under-estimation of the noise current, which can also include effects from many other factors. Thus, a direct comparison in D^* values from different groups and different reports cannot be directly made [16–23].

The same group above also fabricated a highly-patterned $(PMA)_2PbCl_4$ single crystalline microbelt (SCM) array using a similar strategy of space-confined templating [21]. Here, crystal arrays of $(PMA)_2PbCl_4$ perovskite were developed using a polydimethylsiloxane (PDMS) template to facilitate antisolvent crystallization. The micropores confine the solution after being firmly adhered to the substrate, thus restricting the growth to crystal arrays as shown in Fig. 6**a**. The crystallization took place inside the microchannels when anisole vapours diffused into the solution and caused it to become super-saturated. The growth could only proceed preferentially along the microchannels due to the enclosing effect, which caused the direction of the various microbelts (MBs) to be aligned. Then, the PDMS template was removed from the substrate after the entire solvent had evaporated, leaving precisely-aligned MMBs behind. High resolution transmission electron microscopy (HR-TEM) imaging and selected area electron diffraction (SAED) patterns affirm an orthorhombic FE phase with the growth orientation of MB along the [011] direction (Fig. 6**b-c**). Here, the same Bi/ Ag electrode as in their previous work was used as the top and bottom electrodes. After poling, highly-patterned $(PMA)_2PbCl_4$ SCM arrays using the microchannels in the PDMS template were investigated for UV sensing after ensuring the alignment of the perovskite crystals. Under illumination with 320 nm light, the energy band bending effect induced by the FPPE significantly enhanced (photocurrent generation mechanism is explained in Fig. 4) the photo response of the device due to both ferroelectricity and pyroelectricity (Fig. 6**d-e**). The device exhibited a detectivity of 2.3×10^6 Jones and a responsivity of 155.5 mA/W with a very good rise/ fall time of 73/ 52 μs, respectively [21]. However, the photoresponsivity in the SPD using $(PMA)_2PbCl_4$ SCM is less compared to that of $(PMA)_2PbCl_4$ MMB based SPDs. This might be attributed low trap-state density in $(PMA)_2PbCl_4$ MMB than in $(PMA)_2PbCl_4$ SCM due to well-controlled orientation and good crystallinity. As a result, a comparatively better defect free electronic structure

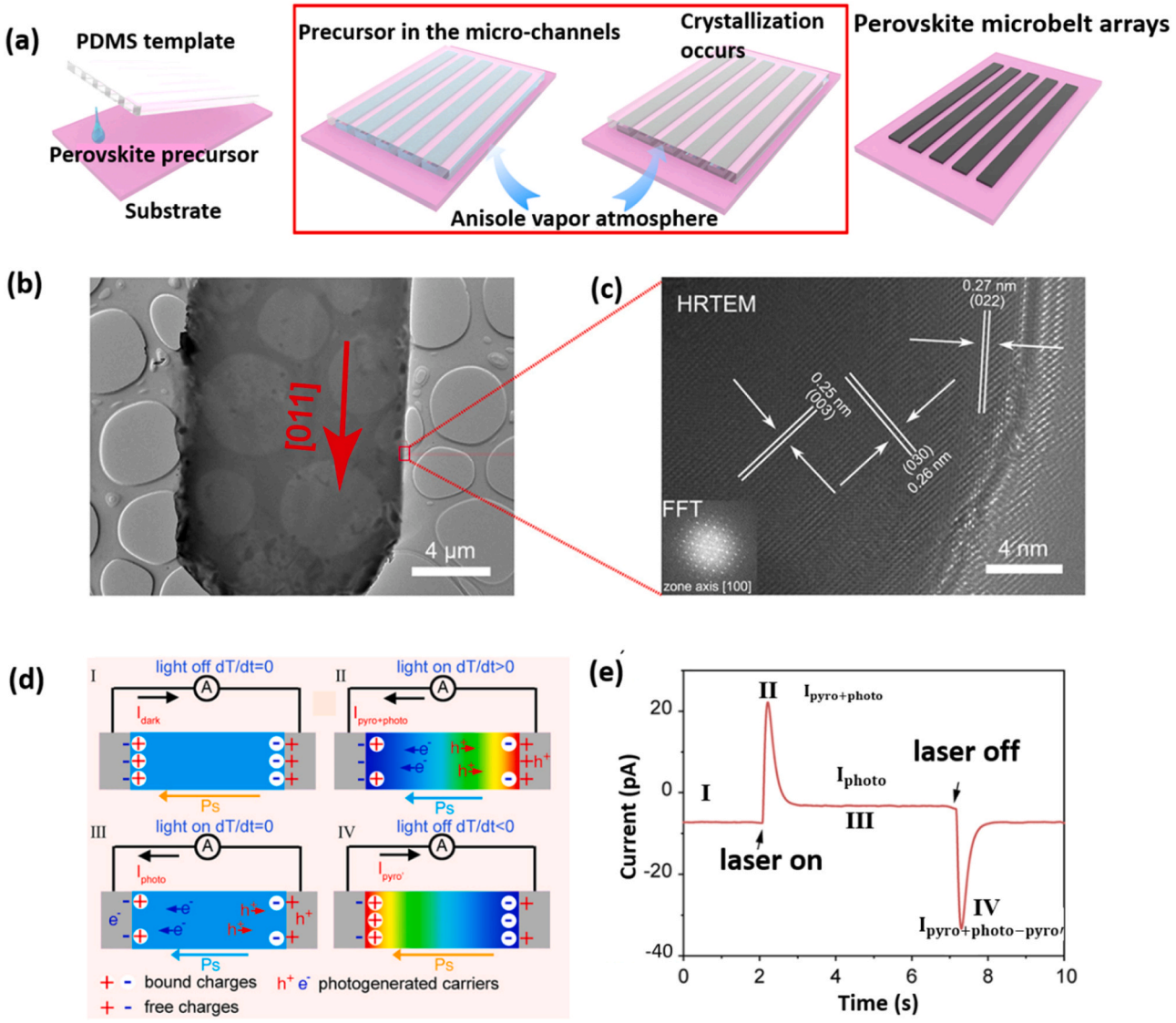

Fig. 6. (a) Growth technique, (b) HR-TEM image, (c) SAED pattern of $(PMA)_2PbCl_4$ SCM, (d) working mechanism using FPPE and (e) corresponding current response in the $(PMA)_2PbCl_4$ SCM under 320 nm UV light illumination. Reproduced with permission [21]. Copyright@ 2022, American Chemical Society Publishing.

and thereby, a higher photoresponsivity.

Yang et al., in 2022 fabricated a self-powered one-dimensional/ three-dimensional (1D/ 3D) heterojunction-based flexible photodetector with a FE 1D $(CH_3)_3NCH_2IPbI_3$ (TMIMPbI$_3$) incorporated into a 3D MAPbI$_3$ perovskite film (3D) [22]. The flexible 1D/ 3D film was prepared using the sol-gel technique and is shown in Fig. 7**a**. The formation of 1D/ 3D flexible films was confirmed using HR- TEM imaging, giving a clear identification of TMIMPbI$_3$ (1D) from the 3D MAPbI$_3$ matrix (perovskite layer) and is shown in Fig. 7**b**. In this work, poly (3-hexylthiophene-2,5-diyl) (P3HT) was used as the p-type layer and the device structure was PEN/ITO/perovskite/P3HT/Ni/Au. The light illumination created a responsivity of 6.6 mA/W and detectivity of 5×10^9 Jones by utilizing the FPPE and the mechanism is shown in Fig. 7**c**. The results can be explained by the mechanisms illustrated in Fig. 4 Thus, under illumination, negative polarization charges from ferroelectricity decreased at the perovskite/P3HT interface which not only favours electron migration from the MAPbI$_3$, but it also drives the holes away from the p-type P3HT. This bends the energy band downwards because of the FPPE. Thus, the modulation of ferroelectric polarization charges on the carrier photoelectric process near the p-n junction interface is a highly consistent explanation for the enhanced performance of 1D/3D ferroelectric perovskite SPD. The self-powered flexible 1D/ 3D PD produced a responsivity of 6.6 mA/ W, a detectivity of 5×10^9 Jones, and a rise/ fall time of 35/36 ms, respectively [22].

Two-dimensional (2D) Ruddlesden–Popper metal-halide perovskites are another class of MHPs getting attention for high performance SPDs. 2D Ruddlesden–Popper (RP) perovskites have the general formula $L_2A_{n-1}M_nX_{3n+1}$. Here, L is a long chain organic cation (spacer), A is a short chain organic cation, M is a divalent metal cation, and X is a halide anion. Usually, the [MX$_6$] inorganic octahedral monolayer is sandwiched between two organic spacer layers. In 2D RP perovskites, the long-chain hydrophobic ligands improve the stability against moisture and oxygen compared to their 3D organic–inorganic hybrid perovskite counterparts [29,30]. Different preparation techniques, such as hot-casting, solvent engineering, and additive engineering, have been developed to control the preferred orientation to ensure the high-mobility inorganic layers connect the electrodes of the vertical structure PD device [29]. This ensures the efficient collection of photogenerated charge-carriers from 2D HPs [30]. Liu et al., in 2022 fabricated a PD using caesium (Cs) based (*n*-hexylammonium) $CsPb_2Br_7$ 2D RP ferroelectric perovskite [31]. The FPPE was enhanced by moulding the interlayer spacers (Fig. 8**a**). The high electric polarization in this 2D RP arises due to the tilting of PbBr$_6$ and the dynamic motion of Cs^+ along with the frozen ordering of the organic spacer (*n*-hexylammonium). Upon illumination with 405 nm wavelength UV light, the device reported a rise/ fall time of about 1.5 and 3.6 s, respectively [31]. The strong performance can be explained by the intensity of the electric dipole vibration increasing with light illumination, promoting electron-hole pair formation at the surface of the ferroelectric. Very recently, Guo et al., reported in 2D RPs, very high responsivity and detectivity in a UV PD via the FPPE [23]. Here, highly crystallized 2D RP $(BA)_2(MA)_{n-1}Pb_nBr_{3n+1}$ (with 'n' ranging from 2 to 5 and named as P2, P3, P4, and P5, respectively) was successfully synthesized by spin-coating. The final device structure is glass/-ITO/$(BA)_2(MA)_{n-1}Pb_nBr_{3n+1}$/ PC61BM/Bi/Ag, as shown in Fig. 8**b**. XRD patterns confirmed the formation of a $(BA)_2(MA)_{n-1}Pb_nBr_{3n+1}$ film with (111) and (202) crystal planes of 2D perovskite (Fig. 8**c**). The structure was further confirmed using grazing-incidence wide-angle X-ray scattering (GIWAXS). Sharp Bragg spots with diffraction peaks of (060), (080), and (0100) indicated a preferred orientation of the crystal perpendicular to the substrate (Fig. 8**d**). A comparatively high crystal structure and strong ferroelectricity were observed for the poled film (P4) and subsequent photocurrent studies were undertaken. During illumination (360 nm), the energy band bent downwards due to reduced negative polarization charges at the 2D perovskite and organic semiconductor ($PC_{61}BM$) interface. This is ascribed to the built-in electric field developed by the light-generated electrons and holes due to the induced ferroelectricity and pyro-phototronic effect (FPPE), as already discussed for the other materials and as shown in Fig. 4. Overall, the glass/ITO/$(BA)_2MA_3Pb_4Br_{13}$/ PC61BM/Bi/Ag device generated a responsivity of 1 A/W and a detectivity of 1.54×10^{14} Jones under a zero-bias voltage [23].

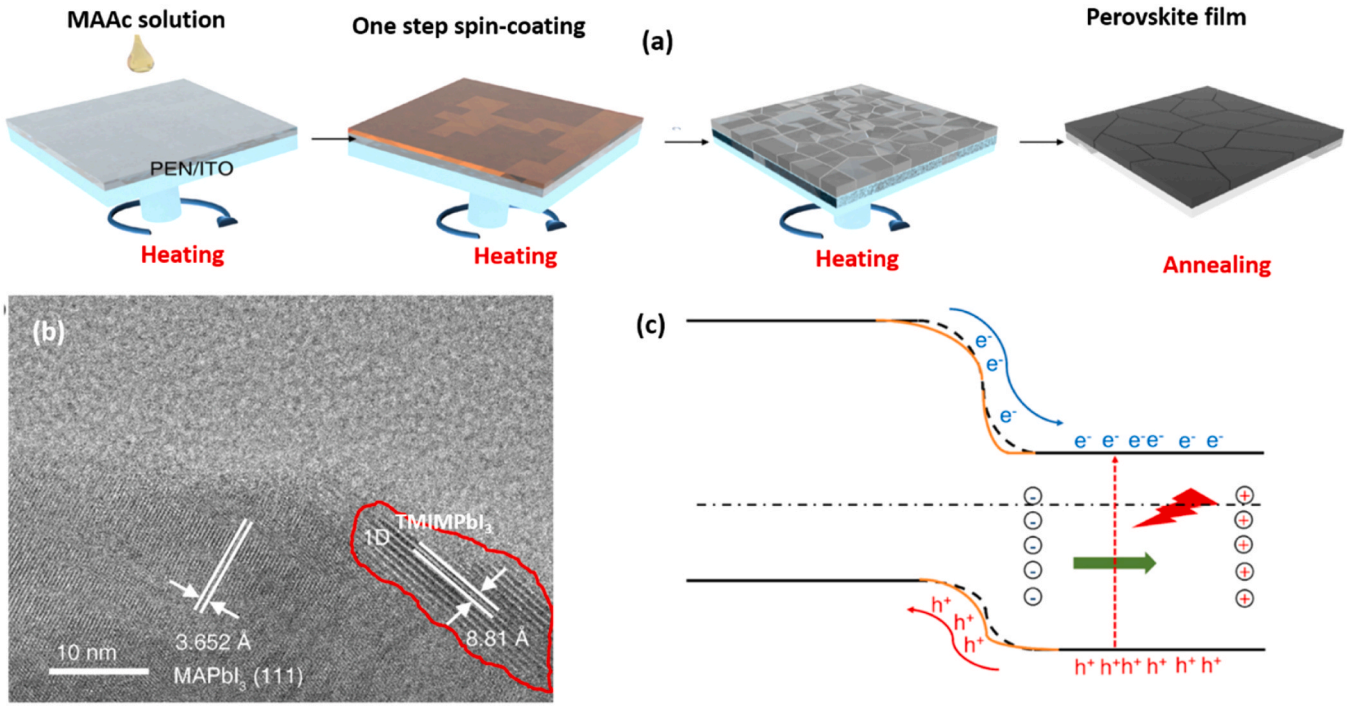

Fig. 7. (a) Schematic representation of growth technique of TMIMPbI$_3$, (b) HR-TEM image of (1D) TMIMPbI$_3$ from the 3D MAPbI$_3$ matrix and (c) working mechanism of the FPPE Effect in PEN/ITO/perovskite/P3HT/Ni/Au device. Reproduced with permission [22]. Copyright@ 2020, Elsevier Publishing.

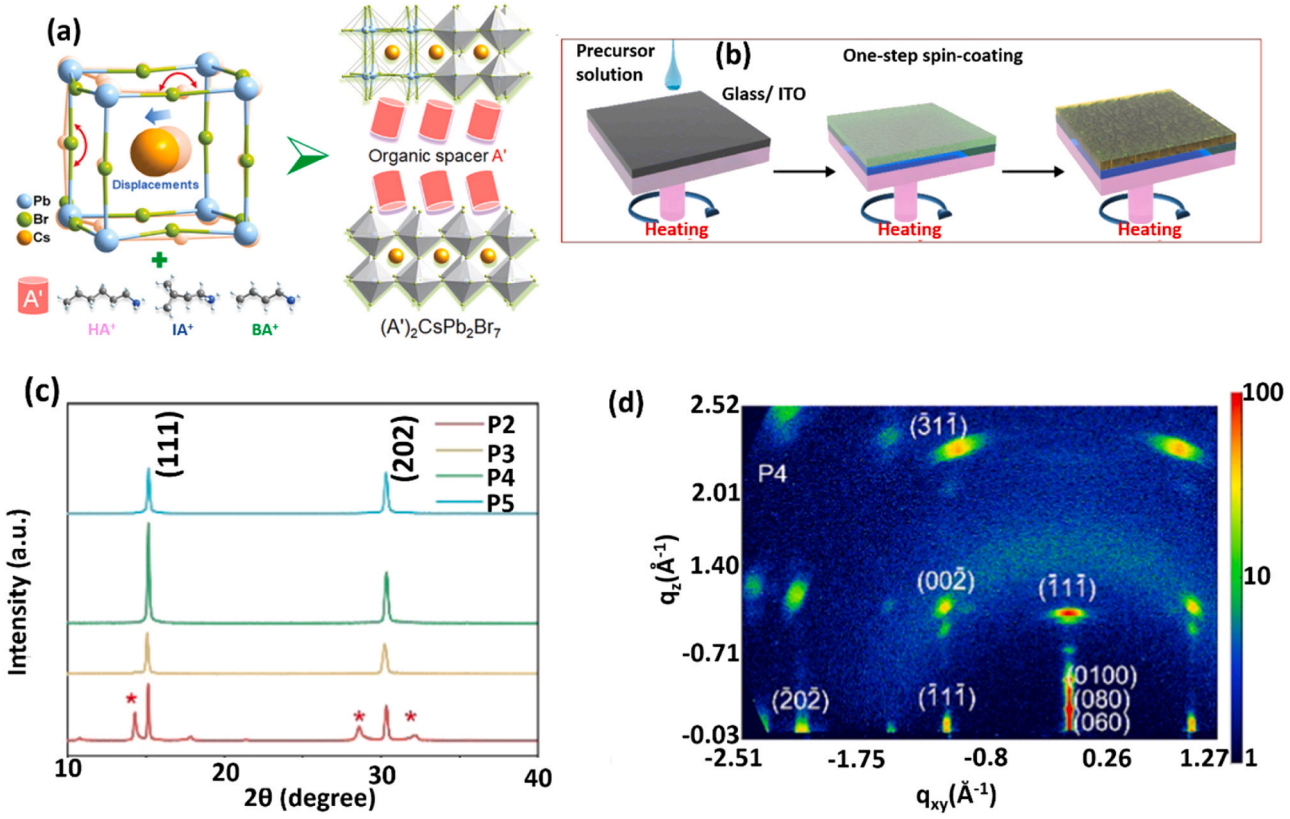

Fig. 8. (a) Diagram showing the customization of interlayered spacers by mixing the organic spacers with the A′ site (A′ = HA^+, IA^+, and BA^+) and inorganic Cs^+. Reproduced with permission [31]. Copyright@ 2022, Wiley Publishing. (b) Fabrication process of 2D Ruddlesden Popper (RP) films of $(BA)_2(MA)_{n-1}Pb_nBr_{3n+1}$ films, (c) XRD pattern of the films (d) GIWAXS image. For the glass/ITO/$(BA)_2(MA)_{n-1}Pb_nBr_{3n+1}$/ PC61BM/Bi/Ag device. Reproduced with permission [23]. Copyright@ 2022, Elsevier Publishing.

3.2. ABO_3 perovskite bulk

In ABO_3 FE bulk ceramics, the depolarization field from intrinsic ferroelectricity (i.e., after poling) leads to the separation of photo-generated electrons and holes due to an enhanced built-in electric field [19]. Furthermore, the remnant polarization has a strong dependence on temperature and can significantly contribute to the pyroelectric current, which is not the case for pyroelectric semiconductors [24]. In 2018, Zhao et al., demonstrated the FPPE effect in FE ceramics for the first time [19] in a BTO ceramic disc-based PD and found enhanced photocurrent. A BTO ceramic disc was synthesized by sintering orthorhombic BTO nanoparticles, as confirmed by XRD (Fig. 9**a**). Planar ITO top and bottom electrodes (ITO/BTO/ITO) were applied and then patterned using a laser engraving method as shown in Fig. 9**b** to give radial polarization in the BTO ceramics. The pyroelectric performance of the radially polarized BTO device was 16 nC/cm^{2}K, which is 7.6 times higher than a vertically structured Ag/BTO/Ag device (2.1 nC/cm^{2}K). Illumination with 365 nm wavelength light and simultaneous heating produced a specific detectivity of 378.8 Jones and a responsivity of 0.0071 mA/W. The responsivity is 117.5 times higher for vertical Ag/BTO/Ag made by the same group, and the enhanced response was attributed to FPPE from simultaneous light-heating/cooling. The appreciable photo current generation was explained using an energy band diagram similar to Fig. 4. Thus the BTO ceramic is sandwiched between two SB interfaces, where positive and negative charges forms at the BTO layer surface after poling, and SB height is adjusted at the electrodes. Electron-hole pair generation from illumination and separation at the left SB interface produces the photocurrent. The separation of the electron-hole pair is increased due to the light illumination because the height of the left SB is reduced by the light-induced heating, which produces a pyroelectric effect which reduces the polarized charge density at the electrode and reduces the SB height. However, the height of the right SB increases, which thereby hinders the electron flow resulting in a weak photocurrent. This weakens the effective electron-hole pair separation. Overall, heating from the light reduces the photocurrent. On the other hand, the cooling of the device upon removal of the illumination increases the photocurrent response. The electron-hole pair separation increases because of an increase in polarized charges arising from the pyroelectric effect, and which increases the height of the left SB interface. At the same time, the height of the SB at the right interface is decreased which therefore promotes electron hole pair separation here. Consequently, the device generates a higher photocurrent plateau compared to the light + heating condition [19].

The work of Zhao et al., paved the way for later exploration of FE ceramic-based SPDs utilizing FPPE [16]. Hence, in 2019 Ma et al., further boosted the photocurrent response in the same ITO/BTO/ITO device using simultaneous light-cooling conditions [24]. Here, planar interdigitated electrodes of ITO were deposited on the BTO ceramic and the device was poled for 30 min at 2.5 kV/cm. The PD was designed to detect a UV light of 405 nm. The photocurrent generation showed a strong dependence on temperature and was ascribed to the height variation of the two ITO/BTO SBs with temperature. At low temperature, the three phenomena namely, photovoltaic, ferroelectric, and pyroelectric effects come into picture. Initially, the UV light stimulates a greater number of electrons, not only through band-to-band transitions, but also by exciting carriers from shallow trap levels. Then, the induced polarization in the BTO layer enhances the depolarization field developing a strong driving force reasonable for more electron-hole pair separation. Finally, the light induced heating effect favours the pyroelectric effect to significantly contribute to the output current generation. However, the high temperature weakens the electron generation from shallow traps and also lowers the depolarization field required for

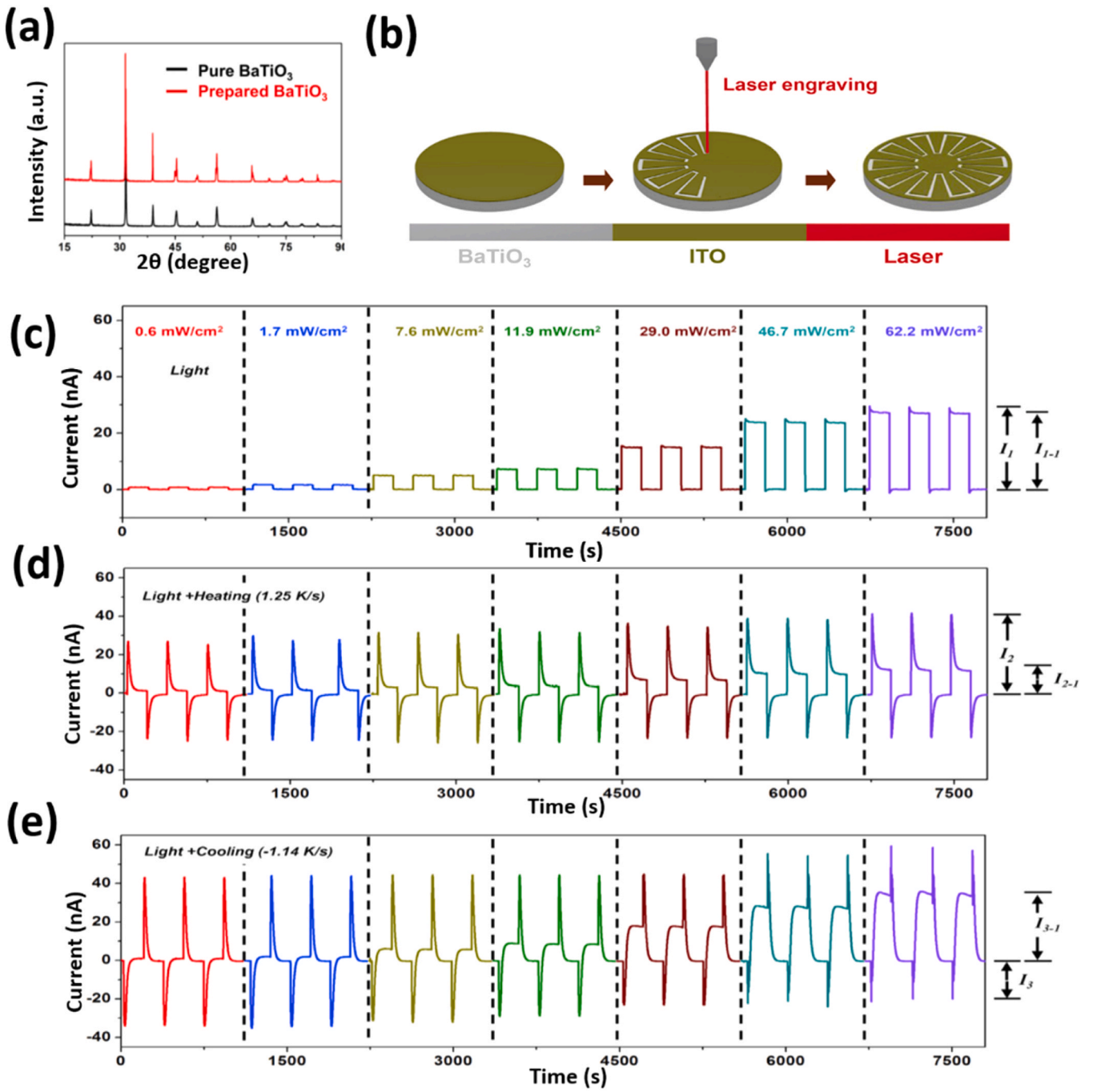

Fig. 9. (a) XRD pattern of BTO nanoparticle precursor ceramic disc before (black) and after (red) sintering, (b) electrode deposition using the laser engraving technique, Measured output current under (c) light alone, (d) light + heating, and (e) light + cooling. Reproduced with permission [19].

electron-hole pair separation. As a result, recombination of electron-hole pairs takes place rather than electron-hole pair separation, and thereby, and the photocurrent is drastically reduced. A maximum detectivity of 0.015 × 10^{10} Jones and a responsivity of 0.0014 mA/W [24] were achieved in the ITO/BTO/ITO device. Furthermore, the co-planar interdigitated ITO electrode in the ITO/BTO/ITO device structure not only reduced the recombination, but also enhanced the charge collection in the photovoltaic process. This might be a reason for higher responsivity in ITO/BTO/ITO device than in ITO/BTO/ITO device (used planar electrodes) fabricated by Zhao et al. A further advance by Zhao et al. in 2020, was to create a flexible Ag/BTO/ITO PD formed of 16 devices on a kapton membrane (Fig. 10**a**) which scavenged both thermal and solar energy via FPPE [32]. The enhancement in the photovoltage upon simultaneous UV light illumination of 405 nm and heating/ cooling conditions (Fig. 10**b-c**) is ascribed to the FPPE mechanism explained using Fig. 4. Zhao et al., have also demonstrated a self-powered multifunctional nanogenerator which senses light, pressure, and temperature [33]. A 3 × 3 sensor array encapsulating ITO/BTO/ITO devices on polydimethylsiloxane (PDMS) was designed to ensure a flexible sensor system. The output current response of the flexible sensor is studied on a prosthetic hand using different sources such as UV light (405 nm), fingertip pressure, and temperature variations (Fig. 10**d-k**). The device was tested under a simultaneous light and ice cooling, and it exhibited an 82.2% enhancement in the output current response compared to individual UV light radiance [33].

Even though BTO ceramic-based PD show good photocurrent

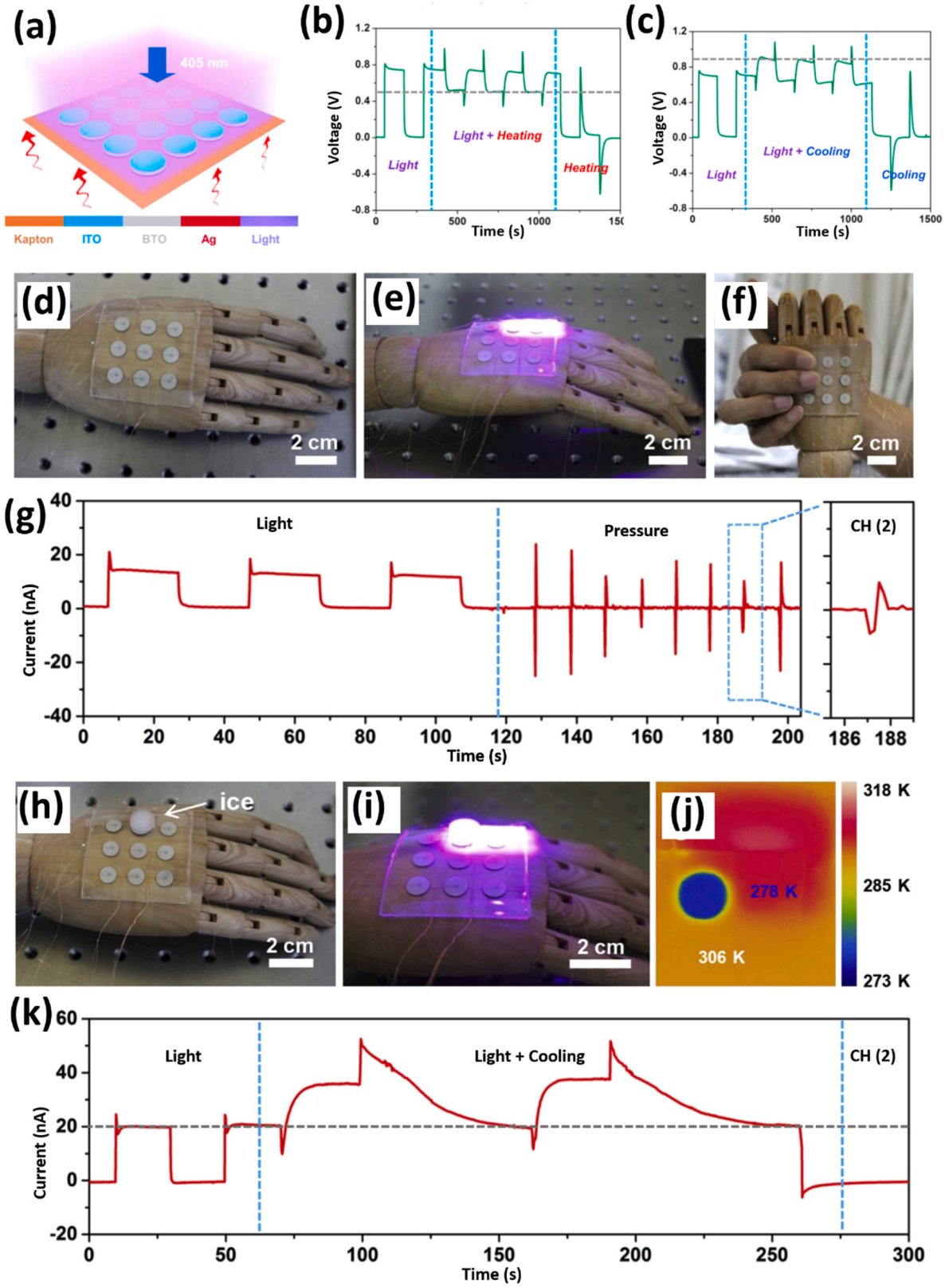

Fig. 10. (a) Representation of Ag/BTO/ITO device characterization, (b) measured voltage under light and heating conditions, (c) measured voltage under light and cooling condition. Reproduced with permission [32]. Copyright@ 2020, Elsevier Publishing. ITO/BTO/ITO devices image (d) flexibility, (e) response to UV illumination, (e) fingertip pressure, and (g) corresponding output current signals as a function of time, image of ITO/BTO/ITO sensor system with (h) ice cooling, (i) ice cooling + light, and (j) IR image showing ice cooling + light, (k) output current response under simultaneous ice cooling + light. Reproduced with permission [33]. Copyright@ 2020, Elsevier Publishing.

response, high temperature PD applications are not possible owing to the ferroelectric-paraelectric phase transition (at the Curie temperature (T_C) of around 120 °C), which means that there is no FFPE above 120 °C [19,25]. Very recently Liu et al., investigated the photocurrent response in $Bi_{0.5}Na_{0.5}TiO_3$ (BNT). which has a T_C of ~350 °C. Ceramic discs were made from BNT nanoparticles by solid state reaction and sintering and metallic electrodes were applied of Ag and ITO to give a Ag/BNT/ITO structured PD device. The device was poled under 1.5 kV/cm at room temperature. A comparison of the performance of the BNT device with the BTO device is made and shown in Fig. 11. The ferroelectric polarization (both remnant and saturation) in the BNT device is maintained at high temperatures, while degraded for BTO device (Fig. 11**a-b**). Thus, Ag/BNT/ITO device draw the possibilities of the enhanced photocurrent response at higher temperatures. The photocurrent generation under heating and cooling at 405 nm light illumination was studied (mechanism is same as Fig. 4) and the response is shown in Fig. 11**c-d**. Polarisation enhanced electron-hole pair separation and electron transport was found [25]. The elevated temperature increases the pyroelectric effect as well as enhancing carrier mobility and hence carrier extraction from the device. The simultaneous application of light and heat augmented the photocurrent peak to a 131% compared to the photocurrent under light irradiation alone at a ΔT of 18. 3 K. Hence, the photocurrent and FPPE both play critical roles [25]. A rise and fall time of 84.2 ms and 54.3 ms, respectively, were achieved which is faster compared to BTO bulk SPDs (seconds range) [25].

3.3. ABO_3 Thin films

ABO_3 ceramics suffer drawbacks such as low photocurrent generation and large response time. Hence, in the former example values of BTO and BNT from the literatures are typical [19,24,25]. Low depolarization field is at least one contributor to this as this provides a low driving force to separate the electron-hole pairs which is necessary to achieve a photocurrent. Another challenge for bulk materials is that a high voltage is necessary to indue FE polarization. Furthermore, larger thickness and crystal boundary of the inorganic ABO_3 bulk can adversely affect the response time [25].

Inorganic FE ABO_3 based thin films, on the other hand, require a comparatively low voltage to stimulate ferroelectricity. Moreover, FE ABO_3 thin films have superior pyroelectric coefficients compared to the commonly used bulk/ thin film ZnO PDs [26]. **This mandates the necessity of developing high quality thin film based pyroelectric FEs to induce superior photocurrent response utilizing the FPPE.** Very recently, Silva et al. fabricated ferroelectric $0.5Ba(Zr_{0.2}Ti_{0.8})O_3$-$0.5(Ba_{0.7}Ca_{0.3})TiO_3$ (BCZT) and demonstrated FPPE in Al/Si/-SiO_x/BCZT/ITO thin film devices and showed the high potential of these

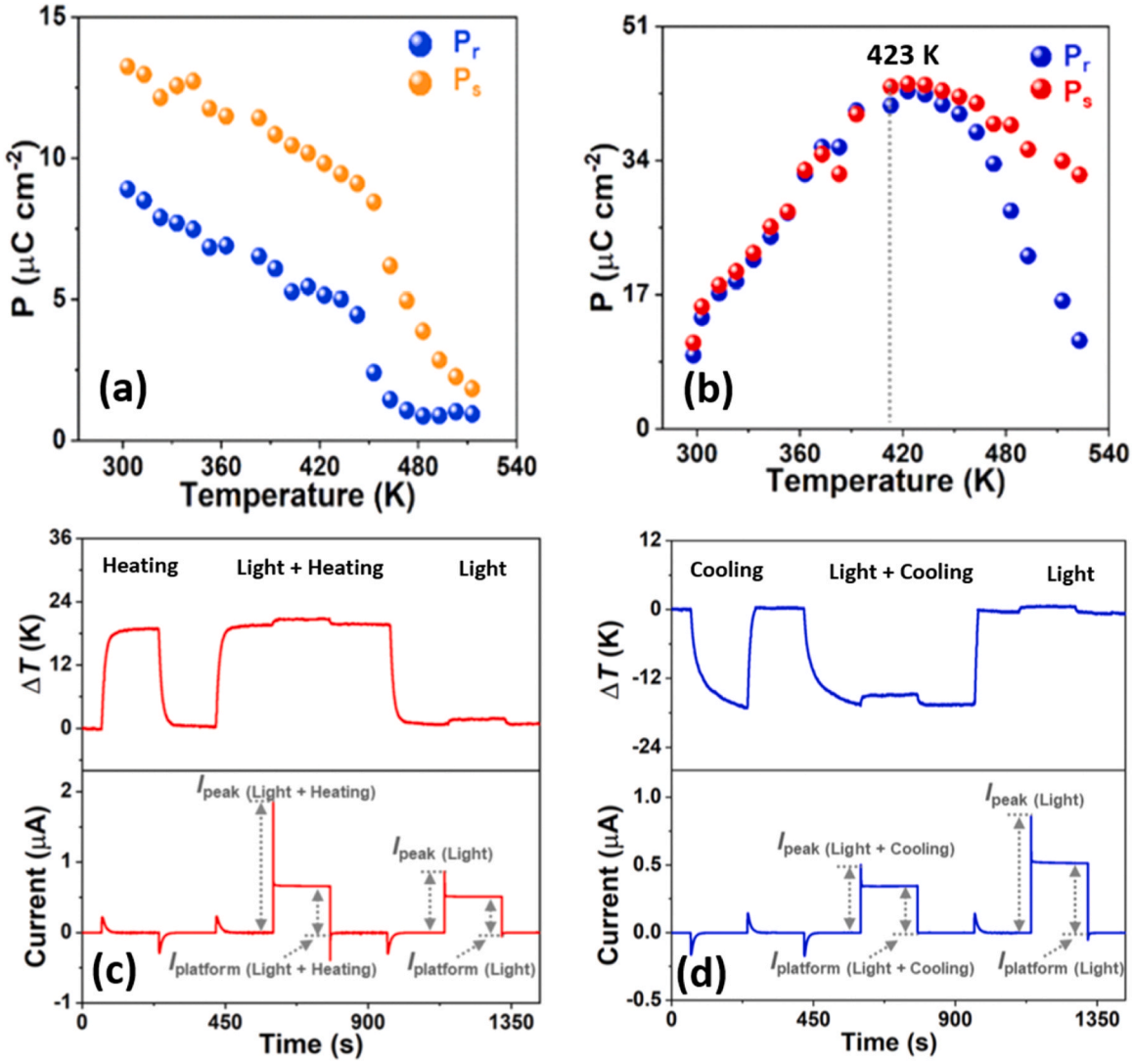

Fig. 11. Temperature dependence of saturation polarization and remanent polarization in (a) Ag/BTO/ITO and (b) Ag/BNT/ITO device, Photocurrent measurement in Ag/BNT/ITO device under (c) light + heating, and (d) light + cooling, respectively. Reproduced with permission [25]. Copyright@ 2022, Elsevier Publishing.

FE based thin films for SPD applications [26]. Tetragonal, ferroelectric phase, films of thickness 80 ± 5 nm were deposited by pulsed laser deposition from a BCZT ceramic target. Here, Si/SiO_x acted as the n-type layer to form a metal-ferroelectric-insulator-semiconductor (MFIS) heterostructure. The current-voltage (I-V) revealed a stable photocurrent response under a laser illumination of 405 nm indicating PPE in the MFIS device. To successfully achieve the FPPE, the Al/Si/-SiO_x/BCZT/ITO thin film device was then poled. Fig. 12**a-b** shows a significant influence of the poling voltage on the PPE. Furthermore, the ferroelectricity in the Al/Si/SiO_x/BCZT/ITO thin film device is confirmed using polarization-voltage curve (Fig. 12**c**). The mechanism constituting the FPPE in the MFIS device with both positive and negative poling is shown in Fig. 12**d-e**. Under a negative poling condition with 405 nm light illumination, the BCZT-induced FE polarization direction causes an increase in SB at the ITO/BCZT interface and thereby, causes a band bending in the upward direction (Fig. 12**d**). At the same time, an upward band bending at the Si surface is observed due to the pyroelectric induced electric field at the Si/BCZT junction. This leads to a higher photocurrent response attributed to the alignment of the depolarization field ($E_{dp-BCZT}$) and pyroelectric field (E_{Pyro}) in the same direction. However, during the positive poling with light illumination, a downward band bending at the ITO/BCZT interface and Si surface occurs (Fig. 12**e**). This is expected due to the electric fields $E_{dp-BCZT}$ and E_{Pyro} being in the opposite direction. Consequently, a reduced photocurrent response was achieved. This shows that the band diagram of the heterostructure, including the SB height, is significantly influenced by polarization-dependent interfacial coupling between ITO and BCZT and between BCZT and SiO_x/Si. Furthermore, the MFIS device demonstrates stability for up to 100 cycles without any performance degradation (Fig. 12**f**). The device showed an excellent responsivity (13.1 mA/W), detectivity (1.7 × 10^{10} Jones) and a rise/ fall time (2.4/ 1.5 μs) compared to inorganic perovskite bulk SPDs [26]. This study therefore demonstrated an ultrafast UV SPD based on an inorganic FE perovskite oxide thin film utilizing its ferroelectricity, pyroelectricity and photoexcitation properties in a MFIS heterostructure.

Furthermore, very recent investigations introduced aurivillius FE materials and new FE semiconductor materials for photo sensing utilizing the FPPE [27,28]. You et al., fabricated an SPD comprising Bi microspheres array and aurivillius $Bi_{3.8}Nd_{0.2}Ti_3O_{12}$ ($Bi@Bi_{3.8}Nd_{0.2}Ti_3O_{12}$) for photodetection [27]. The film was fabricated using the electrospinning method. The high photo response in <ITO/$Bi@Bi_{3.8}Nd_{0.2}Ti_3O_{12}$/Al> device is attributed to the substitution of Bi by Nd at the A-site, which reduces the oxygen vacancies and thereby hinders the pinning effect of the defects on the domain wall. Consequently, the ferroelectric polarization increases due to increased domain wall motion. Moreover, Bi microsphere arrays enhance the light absorption and favours the conversion of temperature fluctuations into electrical energy utilizing ferro-pyro phototronic effect. Consequently, there is an enhancement in the photo response. This <ITO/$Bi@Bi_{3.8}Nd_{0.2}Ti_3O_{12}$/Al> device reported an excellent detectivity (81. 1 × 10^{10} Jones) with a fast rise/ fall time (57/ 114 μs).

Furthermore, Jia et al., introduced a 2D FE semiconductor **α**-In_2Se_3 for the fabrication of SPDs [28]. The work accomplished an outstanding detectivity of 1.6 × 10^{13} Jones with a fast response time of 43 μs. In this work, a 2D **α**-In_2Se_3 was grown on fluorphlogopite mica (F-mica) using atmospheric pressure chemical vapor deposition (APCVD) method. The **α**-In_2Se_3 was then transferred onto n-Si substrate. Finally, a device was fabricated using Ti/Au and In/ Ga alloy as top and bottom electrodes. The intrinsic ferroelectric polarization in **α**-In_2Se_3 modulates the photovoltaic effect by enhancing the recombination activity of the photoexcited charge carriers.

4. Challenges, potential solutions, and future prospects for self-powered photodetectors based on the ferro-pyro-phototronic effect

The most recent advances in FE SPDs utilizing FPPE were reviewed for different types of FE materials such as metal halide perovskites, 2D Ruddlesden–Popper metal halide perovskites, ABO_3 inorganic ceramics and ABO_3 inorganic thin films. While Table 1 shows promising results in terms response time, detectivity and responsivity of FE SPDs, further improvements of these FE materials in terms of structure-wise and performance-wise are needed in order to reach required commercial device performance. Below we consider the challenges and

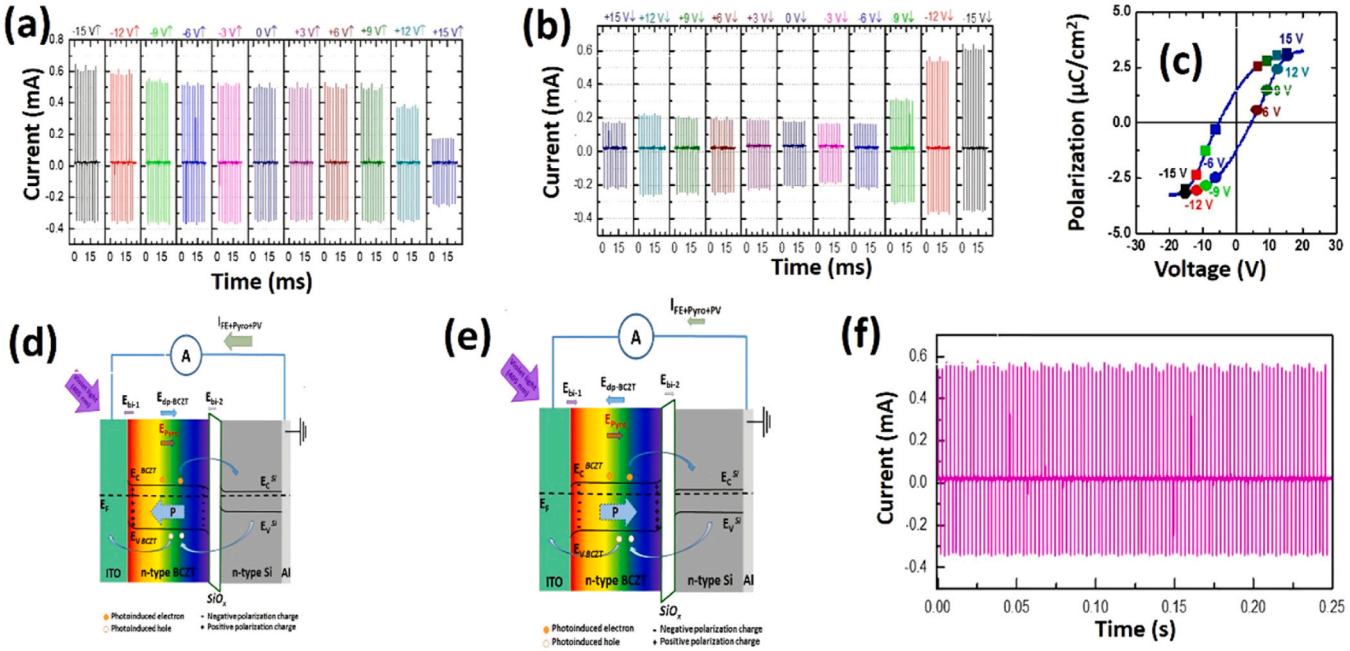

Fig. 12. Ferro-pyro-phototronic effect in Al/Si/SiO_x/BCZT/ITO devices: (a-b) current-time plot at different poling voltages, (c) polarization-voltage curve, working mechanism, schematic structure under light irradiation with simultaneous (d) negative poling voltage and (e) positive poling voltage, (f) stability of the current response under 405 nm laser illumination [26].

opportunities of the different classes of materials and suggest possible new materials for FPPE based SPDs.

4.1. Metal halide-based perovskites

Metal halide-based perovskites (MHPs) possess favourable attributes for SPD applications, including high detectivity, excellent responsivity and good response time [20,21,23]. They are also amenable to deposition on flexible substrates for bendable devices. 2D MHPs have demonstrated exceptional physical properties derived from the quantum confinement effect. Compared to 3D MHPs for SPD applications, 2D Ruddelsen Popper materials have exceptional properties of enhanced environmental stability, large exciton binding energy, and good photophysical properties. However, the UV light and moisture stability and reliability of 3D and 2D MHPs is a huge concern. The long-term UV–Vis light exposure can be improved by controlling vacancy defects and ion migration [13,14]. The moisture stability is related to the organic component and it is being widely investigated using surface-ligand termination, new hydrophobic organic chains or organic/ inorganic chains, encapsulation, perovskite-polymer composites, crystal morphology control, buffer layer additions, passivating of surface flaws. Another problem of MHPs is their low responsivity towards UV–Vis light. To overcome this, MHPs can be combined with UV–Vis active material [13,14]. Also, to promote the photocurrent response (via enhancing charge separation), 2D MHPs can be combined with FEs [13]. Moreover, the MHP device performance is affected by the operating temperature. High temperatures induce different phase transitions in the MHP and hinder the device performance. In addition, there are chances of degradation of the MHP at higher temperatures [13].

Another concern of 2D MHPs is that the best performing systems contain toxic lead (Pb), which is important for achieving materials with the ideal combination of optoelectronic properties for efficient performance. There is a wide ongoing effort to replace Pb with lower-toxicity cations (e.g., Sn^{2+} and Ge^{2+}, heavy pnictogens Bi^{3+} and Sb^{3+}, or transition metal elements such as Cu^{+}). While there is some success in obtaining materials with optoelectronic properties at a comparable level [13], there is still room for improvement, and further efforts are required to identify the key reasons behind the exceptional performance of lead-halide perovskites and identify systematic methods to replicate these properties in nontoxic alternatives [34].

4.2. ABO_3 inorganic FE perovskite

ABO_3 FE inorganic perovskites on the other hand are materials with simple structure, superior spontaneous polarization, high pyroelectric co-efficient, and excellent piezoelectric co-efficient over conventional ZnO nanowire semiconductors, which is beneficial for SPD applications. The inorganic ABO_3 FE devices possess a relatively higher built-in or inner electric field compared to semiconductor/ heterojunction photovoltaic due to enhanced photogenerated charge transport. Furthermore, if we notice, one of the important progresses is the Pb-free inorganic FEs such as BTO and BNT are characterized for SPD applications, which can show a path breaking in the future environmentally friendly optoelectronic devices compared to MHPs. Also, the working mechanism of FPPE in these inorganic FEs materials is fully demonstrated. So, FEs can play a crucial role in photovoltaic energy conversion.

As already mentioned, the challenge of bulk ABO_3 FE ceramic SPDs is their low photocurrents under UV–Vis illumination. Different strategies such as doping, heterostructure formation, and composites should be implemented to maximise the generated output current. Most importantly, other perovskites besides BTO, NBT and BCZT should be explored. $BiFeO_3$ is a well-known multiferroic material with low band gap, and hence is optimum for visible SPDs. It has also been demonstrated as a PVE material, and hence there are possibilities for it to have good FPPE performance [35].

While the performance benefits of epitaxial and polycrystalline thin film FE PDs over bulk FE PDs of having low poling voltage were shown clearly before in films on both hard and flexible substrates [29], [Li et al.,], [35]. However, many inorganic perovskites have large coercive fields (after poling) and illumination leads to the generation of heat due to the lossy nature of domain wall motion. This can reduce the SPD performance with high-power UV illumination [10]. A way to minimize this effect is to use relaxor FEs which have low coercive fields but sufficient remnant polarization [36]. Such relaxors have not yet been widely explored in SPDs, apart from their structural, ferroelectric and energy storage properties, and much more work should be done on, for example, $BiFeO_3$-based relaxors [35,37].

Overall, with further work on relaxor thin films, is the prospect for thin film-based inorganic FE SPDs to be revolutionary in optoelectronic applications in terms of responsivity, detectivity, and response speed.

4.3. Fluorites

A new class of FE binary oxides (BOs) with a fluorite structure, such as hafnium oxide (HfO_2) and zirconium oxide (ZrO_2), have evolved with strong potential in the electronics market [38]. These BOs have also been commercialized for ferroelectric memory devices [39]. The ferroelectricity in these BOs originate from the non-centrosymmetric orthorhombic phase with space group $Pca2_1$, where the relative oxygen ion displacement from the Hf octahedron centre is the root cause to the FE nature [38]. Recent investigations showed ferroelectricity in ZrO_2 and HfO_2 based thin films with a polar rhombohedral phase [38,40,41]. Experiments showed that HfO_2 and ZrO_2-based films exhibit sufficient ferroelectricity even in the ultra-thin film state, when compared to traditional ferroelectric perovskites. These BOs are getting significant attention in areas such as non-volatile memory, field-effect transistors, energy storage, etc [38]. FE BOs also have advantage of complementary metal-oxide semiconductor (CMOS) compatibility.

Exploiting the pyroelectric effect in BOs would open up new opportunities for SPD applications. There have only been a few investigations to validate the pyroelectric properties in HfO_2 and ZrO_2 based systems [40–46], all of them being relatively recent [37–41]. A large pyroelectric co-efficient was measured ($-70\ \mu C/\ Km^2$) in 14 nm -thick La-doped HfO_2 films and in ultra-thin $Hf_{0.5}Zr_{0.5}O_2$ films [43]. The ferroelectric phase was stabilised in 45 nm-thick ZrO_2 film deposited using atomic layer with a pyroelectric co-efficient of $-\ 35\ \mu C/\ Km^2$ [44]. The PPE effect in 10 nm FE HfO_2 films of mixed phases, in $Ag/HfO_2/-SiO_2/Si$ devices, has already been demonstrated in high-performance self-powered sensors for optical readable memory applications [45]. The photodetection performance under IR illumination (940 nm) was very good with responsivity of 60 mA/W and response time of 60 μs [45]. **Thus, we foresee strong possibilities for FPPE enhanced self-powered photodetectors in the BOs.**

The strong promise of BO materials for FPPE stem first from the simplicity of the composition, the high stability of the materials and high Curie temperatures, up to 450 °C, the latter of which increases the chance of the persistence of ferroelectricity and pyroelectricity to high temperatures leading to stable SPDs [38].

However, in BOs, more attention should be given to the stability of the ferroelectric phases (i.e orthorhombic or rhombohedral phases) contained in them. We note that in HfO_2, the rhombohedral phase appears to be less stable than the orthorhombic one. A key problem is that the FE phase is modified to form a non-FE phase under both mechanical and thermal stimuli. However**, achieving strong pyroelectric performance in the FE BOs as is needed in high performance SPDs requires either stable FE orthorhombic or rhombohedral phase.** A stable ferroelectric phase depends on several factors such as dopant level, surface energy, crystallite size, strain, thermal expansion mismatch, interface layer, capping layer, electrode materials, etc [36,43]. To ensure excellent FE phase stability, new strategies should be implemented. For instance, the stability of the FE phase in HfO_2 and ZrO_2 is reduced by the oxygen and carbon impurities during atomic

layer deposition (ALD). Longer use of ozone dosage in ALD significantly reduces the oxygen vacancies and carbon impurities. This reduces the in-plane tensile stress which aids in the stabilisation of the ferroelectric orthorhombic phase. Defect engineering through light ion bombardment is another important tool that allows the enhancement of the FE properties of the films [38,47]. However, the above methods have not yet been demonstrated to produce enhanced SPD behaviour and should be explored in SPD devices in more detail.

Multi-layer formation of BOs with organic and inorganic FEs have been explored in SPDs and have been shown to improve the photocurrent response. For instance, organic solution processable photodetectors (OPDs) have the benefit of low leakage current but they have poor responsivity. On the other hand, high photoresponsivity in P3HT with pristine HfO_2 as the interlayer was shown recently [46]. Here, the interlayer HfO_2 acted as a blocking layer suppressing the electron hole recombination in the active P3HT layer.

Other possible, as yet unexplored, strategies to enhance SPD performance with BOs is to use bilayers of two BOs with different ferroelectric behaviour. Here, **an additional depolarization field can enhance the built-in electric field in the SPD to separate the electrons and holes to give high photocurrent response**.

4.4. Conclusions and future prospects

In conclusion, currently, out of all materials explored so far, the most suitable candidate for SPD applications is ABO_3 inorganic perovskites. Here, the FPPE is a well-established phenomenon and there is room to enhance the photo current performance using relaxor ferroelectrics. Also, there are well established techniques which can be explored to further improve the ferroelectric (and also pyroelectric and piezoelectric) properties in these materials. It is highly promising that thin film FEs on both rigid and flexible substrates can be made with demonstrated high performance self-powered photodetection capabilities via the FPPE, for applications in nanoscale UV–Vis SPD, e. g wireless communication and defence technology [32,33].

Of the other materials explored, FE MHP-based SPDs show strong detectivity and responsivity performance but have stability issues (against UV illumination, humidity, and temperature) and the presence of toxic Pb are major drawbacks. Most of the high performance MHP SPDs use the toxic element Pb. Works are still ongoing to enhance the stability of MHPs and to replace Pb. FE fluorites show very strong ferroelectric and pyroelectric properties and also have simple structures, but they are still at an under-developed stage in the fabrication of SPDs. Furthermore, combining pyroelectric and PVE using FE BOs has not been explored yet, and hence the FPPE is not yet demonstrated or understood.

It will be important to achieve SPDs for sensing in the visible and IR regions, and lowering the band gap of perovskites will be an important future path to follow in order to enable this. Also, for next generation multi-functional sensory systems, SPD coupled energy harvesters could play a crucial role. In addition, the role of flexible FE SPDs could significantly broaden the scope of flexible nano systems, especially e-skin, wearable electronics, etc. The design and fabrication of FE SPDs that function not only as detectors or sensors but also as flexible batteries or hybrid super capacitors is also an important area for the future. Last but not the least, more focused efforts on FPPE gives strong prospects for FE SPDs to be used in the near future in real-time practical applications such as human-artificial intelligence interactions, space technology, missile technology, medical science, etc.

CRediT authorship contribution statement

Ampattu Ravikumar Jayakrishnan: Date curation, Formal analysis, Investigation, Methodology, Writing – original draft. **José P. B. Silva:** Date curation, Formal analysis, Investigation, Methodology, Conceptualization, Project administration, Supervision, Funding acquisition, Writing – review & editing. **Katarzyna Gwozdz:** Date curation, Formal analysis, Investigation, Methodology, Writing – review & editing. **Maria J. M. Gomes:** Methodology, Funding acquisition, Writing – review & editing. **Robert L. Z. Hoye:** Funding acquisition, Writing – review & editing. **Judith L. MacManus-Driscoll:** Funding acquisition, Writing – review & editing.

Declaration of Competing Interest

The authors declare that they have no known competing financial interests or personal relationships that could have appeared to influence the work reported in this paper.

Data Availability

Data will be made available on request.

Acknowledgement

This work was supported by: (i) the Portuguese Foundation for Science and Technology (FCT) in the framework of the Strategic Funding Contracts UIDB/04650/2020, (ii) exploratory project 2022.01740. PDTC and (iii) the project M-ERA-NET3/0003/2021 - NanOx4EStor grant agreement No 958174 (https://doi.org/10.54499/M-ERA-NET3/0003/2021). J. P. B. S. also thanks FCT for the contract under the Institutional Call to Scientific Employment Stimulus – 2021 Call (CEECINST/00018/2021). JLM-D. and R.L.Z.H. thank EPSRC CAM-IES grant EP/P007767/. R.L.Z.H. also acknowledges support from the Royal Academy of Engineering under the Research Fellowships scheme (No.: RF\201718\1701). J.L.M-D. acknowledges support from the Royal Academy of Engineering Chair in Emerging Technologies scheme (No.: CIET1819_24) and the ERC Advanced Grant, ERC-ADG #882929 EROS. K. G. acknowledges support from the National Science Centre in Poland Grant No. 2023/07/X/ST7/00073.

Appendix A. Supporting information

Supplementary data associated with this article can be found in the online version at doi:10.1016/j.nanoen.2023.108969.

References

[1] H. Chen, K. Liu, L. Hu, A.A. Al-Ghamdi, X. Fang, Mater. Today 18 (2015) 493–502.
[2] P.C. Eng, S. Song, B. Ping, Nanophotonics 4 (2015) 277–302.
[3] W. Tian, Y. Wang, L. Chen, L. Li, Small 13 (2017), 1701848.
[4] X. Hu, X. Li, G. Li, T. Ji, F. Ai, J. Wu, E. Ha, J. Hu, Adv. Funct. Mater. 31 (2021), 2011284.
[5] H. Qiao, Z. Huang, X. Ren, S. Liu, Y. Zhang, X. Qi, H. Zhang, Adv. Opt. Mater. 8 (2020), 1900765.
[6] ⟨https://www.fortunebusinessinsights.com/industry-reports/internet-of-things-iot-market-100307⟩.
[7] M.F. Al Fattah, A.A. Khan, H. Anabestani, M.M. Rana, S. Rassel, J. Therrien, D. Ban, Nanoscale 13 (2021) 15526–15551.
[8] J. Liu, G. Faulkner, B. Choubey, S. Collins, D.C. O'Brien, IEEE Sens. J. 18 (2018) 5321–5328.
[9] V. Panwar, S. Nandi, M. Majumder, A. Misra, J. Mater. Chem. C. 10 (2022) 12487–12510.
[10] S. Sahare, P. Ghoderao, M.K. Sharma, M. Solovan, R. Aepuru, M. Kumar, Y. Chan, Z. Ziółek, S.L. Lee, Z.H. Lin, Nano Energy 107 (2023), 108172.
[11] J.P. Silva, E.M. Vieira, K. Gwozdz, A. Kaim, L.M. Goncalves, J.L. MacManus-Driscoll, R.L. Hoye, M. Pereira, Nano Energy 89 (2021), 106347.
[12] S. Tian, B. Li, Y. Dai, Z.L. Wang, Mater. Today (2023), https://doi.org/10.1016/j.mattod.2023.07.001.
[13] C.P. Veeramalai, S. Feng, X. Zhang, S.V.N. Pammi, V. Pecunia, C. Li, Photonics Res 9 (2021) 968–991.
[14] G. Li, Y. Wang, L. Huang, W. Sun, ACS Appl. Electron. Mater. 4 (2022) 1485–1505.
[15] A.R. Jayakrishnan, A. Kumar, S. Druvakumar, R. John, M. Sudeesh, V.S. Puli, J. P. Silva, M.J. Gomes, K.C. Sekhar, J. Mater. Chem. C. 11 (2023) 827–858.
[16] Z.L. Wang, Nano Today 5 (2010) 540–552.
[17] Z.L. Wang, W. Wu, Natl. Sci. 1 (2014) 62–90.
[18] B. Dai, G.M. Biesold, M. Zhang, H. Zou, Y. Ding, Z.L. Wang, Z. Lin, Chem. Soc. Rev. 50 (2021) 13646–13691.
[19] K. Zhao, B. Ouyang, Y. Yang, Iscience 3 (2018) 208–216.

[20] L. Guo, X. Liu, L. Gao, X. Wang, L. Zhao, W. Zhang, S. Wang, C. Pan, Z. Yang, ACS nano 16 (2022) 1280–1290.
[21] L. Guo, X. Liu, R. Cong, L. Gao, K. Zhang, L. Zhao, X. Wang, R.N. Wang, C. Pan, Z. Yang, Nano Lett. 22 (2022) 8241–8249.
[22] Z. Yang, X. Li, L. Gao, W. Zhang, X. Wang, H. Liu, S. Wang, C. Pan, L. Guo, Nano Energy 102 (2022), 107743.
[23] L. Guo, Y. Qi, Z. Yang, L. Zhao, W. Zhang, X. Wang, H. Liu, G. Yan, S. Wang, C. Pan, Nano Energy 102 (2022), 107714.
[24] N. Ma, Y. Yang, Nano Energy 60 (2019) 95–102.
[25] Y. Liu, Y. Ji, Y. Xia, L. Wu, C.R. Bowen, Y. Yang, Nano Energy 98 (2022), 107312.
[26] J.P. Silva, K. Gwozdz, L.S. Marques, M. Pereira, M.J. Gomes, J.L. MacManus-Driscoll, R.L. Hoye, Carbon Energy 5 (2023), e297.
[27] D. You, R. Wang, L. Liu, J. Peng, Z. Ren, C. Xu, Nano Energy 110 (2023), 108330.
[28] C. Jia, S. Wu, J. Fan, C. Luo, M. Fan, M. Li, L. He, Y. Yang, H. Zhang, ACS nano 17 (2023) 6534–6544.
[29] R.L. Hoye, J. Hidalgo, R.A. Jagt, J.P. Correa-Baena, T. Fix, J.L. MacManus-Driscoll, Adv. Energy Mater. 12 (2022), 2100499.
[30] C. Liang, H. Gu, Y. Xia, Z. Wang, X. Liu, J. Xia, S. Zuo, Y. Hu, X. Gao, W. Hui, L. Chao, Nat. Energy 6 (2021) 38–45.
[31] Y. Liu, X. Pan, X. Liu, S. Han, J. Wang, L. Lu, H. Xu, Z. Sun, J. Luo, Small 18 (2022), 2106888.
[32] K. Zhao, B. Ouyang, C.R. Bowen, Y. Yang, Nano Energy 77 (2020), 105152.
[33] K. Zhao, B. Ouyang, C.R. Bowen, Z.L. Wang, Y. Yang, Nano Energy 71 (2020), 104632.
[34] A.M. Ganose, D.O. Scanlon, A. Walsh, R.L. Hoye, Nat. Commun. 13 (2022) 4715.
[35] Z. Li, Y. Zhao, W. Li, Y. Peng, W. Zhao, Z. Wang, L. Shi, W. Fei, J. Mater. Chem. A 10 (2022) 8772–8783.
[36] A.R. Jayakrishnan, J.P.B. Silva, K. Kamakshi, D. Dastan, V. Annapureddy, M. Pereira, K.C. Sekhar, Prog. Mater. Sci. 132 (2022), 101046.
[37] H. Pan, S. Lan, S. Xu, Q. Zhang, H. Yao, Y. Liu, F. Meng, E.J. Guo, L. Gu, D. Yi, X. Renshaw Wang, Science 374 (2021) 100–104.
[38] J.P. Silva, K.C. Sekhar, H. Pan, J.L. MacManus-Driscoll, M. Pereira, ACS Energy Lett. 6 (2021) 2208–2217.
[39] Ferroelectric Memory Company (⟨ferroelectric-memory.com⟩).
[40] J.P. Silva, R.F. Negrea, M.C. Istrate, S. Dutta, H. Aramberri, J. Íñiguez, F. G. Figueiras, C. Ghica, K.C. Sekhar, A.L. Kholkin, ACS Appl. Mater. Interfaces 13 (2021) 51383–51392.
[41] V. Lenzi, J.P. Silva, B. Šmíd, V. Matolín, C.M. Istrate, C. Ghica, J.L. MacManus-Driscoll, L. Marques, Energy Environ. Mater. (2022) 12500.
[42] P.D. Lomenzo, R. Alcala, C. Richter, S. Li, T. Mikolajick, U. Schroeder, Appl. Phys. Lett. 119 (2021), 112903.
[43] P.D. Lomenzo, S. Jachalke, H. Stoecker, E. Mehner, C. Richter, T. Mikolajick, U. Schroeder, Nano Energy 74 (2020), 104733.
[44] B. Xu, L. Collins, K.M. Holsgrove, T. Mikolajick, U. Schroeder, P.D. Lomenzo, ACS Appl. Electron. Mater. 5 (2023) 2288–2295.
[45] M. Kumar, H. Seo, Adv. Mater. 34 (2022), 2106881.
[46] C.H. Ji, J.Y. Lee, K.T. Kim, S.Y. Oh, RSC Adv. 9 (2019) 29993–29997.
[47] S. Kang, W.S. Jang, A.N. Morozovska, O. Kwon, Y. Jin, Y.H. Kim, H. Bae, C. Wang, S.H. Yang, A. Belianinov, S. Randolph, Science 376 (2022) 731–738.

Ampattu Ravikumar Jayakrishnan is working as a postdoctoral fellow at Centre of Physics of University of Minho and Porto (CF-UM-UP). Prior to this, he was an Assistant Professor in Physics at Sree Narayana Guru College of Advanced Studies, Nangiarkulangara, Alappuzha, Kerala, India. He received his PhD degree in the department of Physics, Central University of Tamil Nadu, India in 2021. He was also a postdoctoral fellow in the Centre for Nanoscience and Engineering, Indian Institute of Science, India. His research interests are ferroelectric energy storage and ferroelectric energy harvesting materials.

José P. B. Silva (ORCID 0000–0002–3485–7032) is an assistant researcher at Centre of Physics of University of Minho and Porto (CF-UM-UP). He graduated in Physics and Chemistry in 2008 and received his Ph.D in 2013 from the University of Minho (Portugal). Between 2014 and 2019, he was a Postdoctoral Fellow at the Materials Physics Institute of the University of Porto (IFIMUP) and at CF-UM-UP, both in Portugal, while between 2019 and 2023, he was a junior researcher at CF-UM-UP. His current research interests focuses on understanding the relationship between structure and functionality of ferroelectric oxide thin films for memory and energy harvesting as well as energy storage applications.

Katarzyna Gwóźdź received her PhD degree at Wrocław University of Science and Technology in 2020. She is currently an Assistant Professor at Department of Quantum Technologies, Wrocław University of Science and Technology. Her main research interests include current transport and point defects in semiconductors, novel materials for photovoltaic applications and implementation of plasmonics in solar cells.

Maria J. M. Gomes is Professor at the Physics Department of the University of Minho. She obtained the PhD from the University of Louis Pasteur, Strasbourg, France in 1990. She worked for more than 25 years on thin films technology, namely in the ferroelectric and semiconductor materials. Her current research interests includes the fabrication and physical properties of lead-free ferroelectric thin films.

Robert Hoye is an Associate Professor at the University of Oxford. He obtained his PhD at the University of Cambridge (2012–2014), followed by a postdoctoral position at MIT (2015–2016), and research fellowships at the University of Cambridge (2016–2019). Subsequently, he moved to Imperial College London as a Lecturer in Jan. 2020, and was proposed to Senior Lecturer in Aug. 2022, before moving to Oxford in Oct. 2022. His research focusses on defect-tolerant semiconductors, and their development into optoelectronic devices, including energy harvesting for Internet of Things applications.

Judith MacManus-Driscoll is Professor in the Materials Science at the University of Cambridge. She is also Royal Academy of Engineering Chair in Emerging Technologies. She is fellow of IOP, IOM3, WES, APS, MRS, and the Royal Academy of Engineering. Her research work is in the area of oxide thin film engineering for low power IT and energy devices. She is interested in both understanding of basic functionalities and in engineering new interfacial-driven properties. For this purpose, she designs, fabricates and analyses novel nanostructured films.